eLife

Neuroscience
Computational and Systems Biology

Dynamic organization of visual cortical networks inferred from massive spiking datasets

Reviewed Preprint
v2 • October 9, 2024
Revised by authors

Reviewed Preprint
v1 • April 4, 2024

Colin Graber, Yurii Vlasov, Alexander Schwing

University of Illinois Urbana Champaign, Department of Electrical and Computer Engineering, Urbana, United States

Abstract

Complex cognitive functions in a mammalian brain are distributed across many anatomically and functionally distinct areas and rely on highly dynamic routing of neural activity across the network. While modern electrophysiology methods enable recording of spiking activity from increasingly large neuronal populations at a cellular level, development of probabilistic methods to extract these dynamic inter-area interactions is lagging. Here, we introduce an unsupervised machine learning model that infers dynamic connectivity across the recorded neuronal population from a synchrony of their spiking activity. As opposed to traditional population decoding models that reveal dynamics of the whole population, the model produces cellular-level cell-type specific dynamic functional interactions that are otherwise omitted from analysis. The model is evaluated on ground truth synthetic data and compared to alternative methods to ensure quality and quantification of model predictions. Our strategy incorporates two sequential stages – extraction of static connectivity structure of the network followed by inference of temporal changes of the connection strength. This two-stage architecture enables detailed statistical criteria to be developed to evaluate confidence of the model predictions in comparison with traditional descriptive statistical methods. We applied the model to analyze large-scale in-vivo recordings of spiking activity across mammalian visual cortices. The model enables the discovery of cellular-level dynamic connectivity patterns in local and long-range circuits across the whole visual cortex with temporally varying strength of feedforward and feedback drives during sensory stimulation. Our approach provides a conceptual link between slow brain-wide network dynamics studied with neuroimaging and fast cellular-level dynamics enabled by modern electrophysiology that may help to uncover often overlooked dimensions of the brain code.

eLife Assessment

The authors describe a model for tracking time-varying functional connectivity between neurons from multi-electrode spike recordings. This is an interesting and potentially **useful** approach to an open problem in neural data analysis, and could be an essential tool for investigating the neural code from large-scale in-vivo recordings of spiking activity. However, the evidence is **incomplete**: systematic comparisons with existing methods and/or demonstration of its utility relative to conventional methods are essential to demonstrate the usefulness of the method.

https://doi.org/10.7554/eLife.95449.2.sa3

Introduction

Information processing in a mammalian brain is distributed across many anatomically and functionally distinct areas[1]. The inter-areal functional and anatomical connectivity can be reconstructed using electron microscopy[2], gene co-expression[3], projection tracing methods[4,5], and functional neuro-imaging[6]. Further analysis of the temporal variation of neural activity across this connectome[7] using functional neuroimaging[8–11] have indicated that complex cognitive functions rely on highly dynamic routing of neural activity within this anatomically constrained structural backbone[12]. Neuroimaging, however, captures activity averaged over large populations (over 500K neurons per voxel) at relatively slow time scales (minutes to hours) that typically shows relatively low dimensionality[13] hence hindering mechanistic explanation. Further insights into dynamic routing of information flows across the brain are expected with adoption of recent technological advances in multielectrode arrays[14,15] and volumetric 2-photon imaging[16] that enable simultaneous recording from large neuronal populations at a cellular level with single spike temporal resolution that reveals rich and high-dimensional dynamic interactions[17,18]. Descriptive statistical approaches[15,19] that summarize the pairwise millisecond-timescale synchrony of spiking within recorded neuronal population indicate a directional flow of functional connectivity[15] ascending along the anatomical hierarchy[5] and reveal distinct engaged modules across the cortical hierarchy[19–21]. However, both descriptive statistical[15,19] as well as modern probabilistic models[22–24] typically extract interactions as time-independent “static” variables[15,19,25] or consider temporal dynamics of the whole population[20,21,26–29]. Temporal changes in the magnitude of pair-wise correlations calculated with descriptive statistical methods have been used to track the dynamics of synaptic interactions during behavior and formation of place fields in hippocampal networks[30–32]. Temporal fluctuations of the synaptic efficacy were also inferred from pair-wise correlations in spike trains using various extended generalized linear models (GLM)[33–37]. However, the synaptic efficacy is typically calculated separately for each neuron pair while in brain networks each neuron is connected to thousands of others.

Here, to uncover the dynamic routing of information in cortical networks, we develop an unsupervised probabilistic model - Dynamic Network Connectivity Predictor (DyNetCP). As opposed to previous approaches that focus on extracting pair-wise correlations[30–37], we aim at learning dynamic changes in connection strength for all recorded neurons in the network. Our approach is also fundamentally different from most of latent variable models that infer the dynamics of the entire recorded population in a low-dimensional latent feature space[26–29].

Instead, to enable interpretation as directed time-dependent network connectivity across distinct cellular-level neuronal ensembles, DyNetCP extracts latent variables that are assigned to individual neurons.

Model

Model architecture

Classical machine learning approaches like variational autoencoders[26,38] successfully train dynamic models of brain activity across entire recorded neural population. However, development of such dynamic models to uncover cellular-level dynamic connectivity structure, is facing a major problem of the virtual absence of ground-truth (GT) data either as verified experimental or synthetic datasets with known time-varying connectivity. In this situation optimization of the model hyper-parameters, control of overfitting, and model verification is largely becoming a surmise. Therefore, to address this challenge, here, learning of the directed dynamic cellular-level connectivity structure in a network of spiking neurons is divided into two stages (**Fig.1A**). First stage, the static component, infers the static connectivity weight matrix $\mathbf{W_{st}}$ (**Fig.1A**, left) via a generalized linear model (GLM). At this stage, the classical descriptive statistical approaches like pair-wise jitter-corrected cross-correlograms[15,30] can be used as a GT to verify the model performance. Next, in the second stage, $\mathbf{W_{st}}$ is used to influence the dynamic offset weight term $\mathbf{W_{off}}$ learned via a recurrent long-short-term-memory (LSTM) algorithm (**Fig.1A**, right). The final dynamic weight $\mathbf{W_{dyn}} = \mathbf{W_{st}} + \mathbf{W_{off}}$ is averaged across all trials. At this stage, the model $\mathbf{W_{dyn}}$ can be verified against another classical descriptive statistical method - pairwise Joint Peristimulus Time Histogram[39] (JPSTH) that represents the time variation of joint correlations. Therefore, dividing the problem into two stages enables independent verification of static weights and dynamic offsets against GT synthetic and experimental data as well as a direct comparison of DyNetCP performance to existing models.

The model operates on trial-aligned binned neural spikes. We collect N neurons recorded for T time bins binned at d bin width across M trials in tensor $X \in \{0,1\}^{M\times N\times T}$, where each entry $x_j^t(i) \in \{0,1\}$ represents the presence or absence of a spike from neuron j at time t in trial i. The spiking probability $P(x_i^t = 1|x^{t-M:t})$ of neuron i at time t is modelled as follows:

$$P\left(x_i^t = 1|x^{t-M:t}\right) = \sigma\left(\underbrace{E_{static}\left(x_i^t|x^{t-M:t}, W_{st}\right)}_{Static} + \underbrace{E_{dyn}\left(x_i^t|x^{t-M:t}, W_{off}\right)}_{Dynamic}\right) \qquad \text{Eq.1}$$

where σ is the sigmoid function, $E_{static} \in \mathbb{R}$ and $E_{dyn} \in \mathbb{R}$ are static and dynamic connectivity logits depending on the trainable weight matrix $\mathbf{W_{st}}$ and the dynamic offset model $\mathbf{W_{off}}$ respectively. Given spiking data as input, the model produces two sets of output weight matrices. The first set, $\mathbf{W_{st}}$, encodes an estimate of the static network structure and contains one weight per pair of neurons averaged across the trial time. These represent the time-averaged influence the spikes of the whole population have on spiking probability of a given neuron. The second set, $\mathbf{W_{dyn}}$, contains a single weight for every pair of neurons for every point in time during the experimental trial. These weights, which are a function of the input spiking data of all neurons in a population, represent a time-varying offset to the static weights. Hence, they encode temporal changes in activity patterns, and are used to determine when a given connection is being active and when it is unused. Therefore, in this formulation, the model learns time-varying connectivity patterns that can be directly linked to the underlying network structure at a cellular level.

Static connectivity inference

The static component of DyNetCP (**Fig.1A**, left), i.e.,

$$E_{static}\left(x_i^t|x^{t-M:t}, W_{st}\right) = \left[\sum_{j=1}^{N}\sum_{d=1}^{M} w_{j\to i}^{d} x_j^{t-d} + b_i\right] \qquad \text{Eq.2}$$

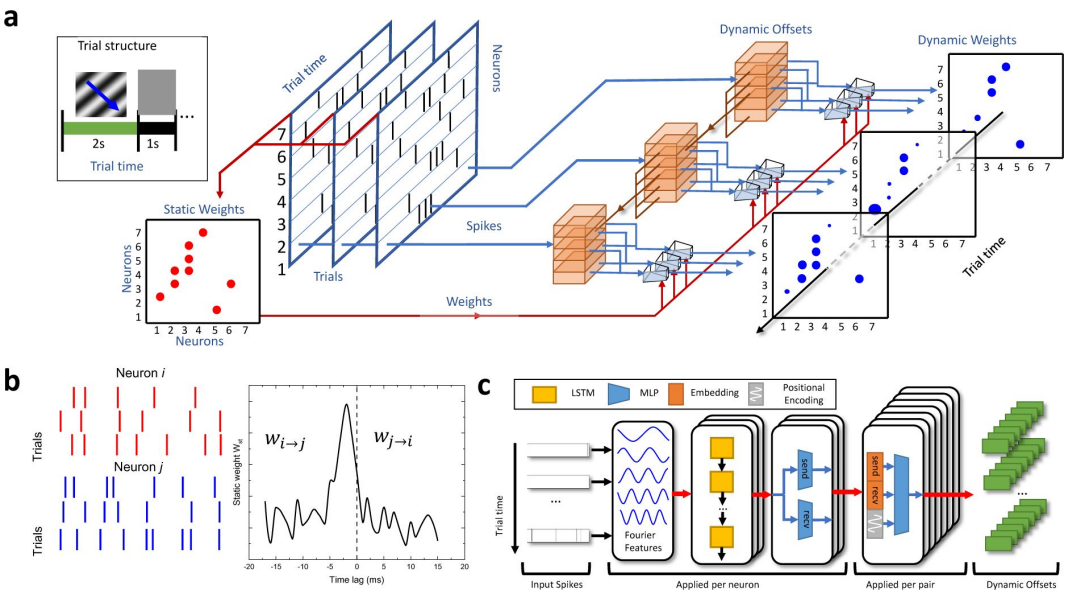

Figure 1.

Model architecture and components design

A) Two-stage model architecture consisting of a static and a dynamic part. **Inset:** structure of the “drifting grating” visual stimulation trial. **B)** Schematics of spike trains recorded from neuron *i* and neuron *j* for three trials and corresponding output of the static part of the model $\mathbf{W_{st}}$. **C)** Schematics of the dynamic part of the mode consisting of a Fourier features transformation, followed by recurrent long-short-term-memory model, multilayer perceptron, embedding, and positional encoding.

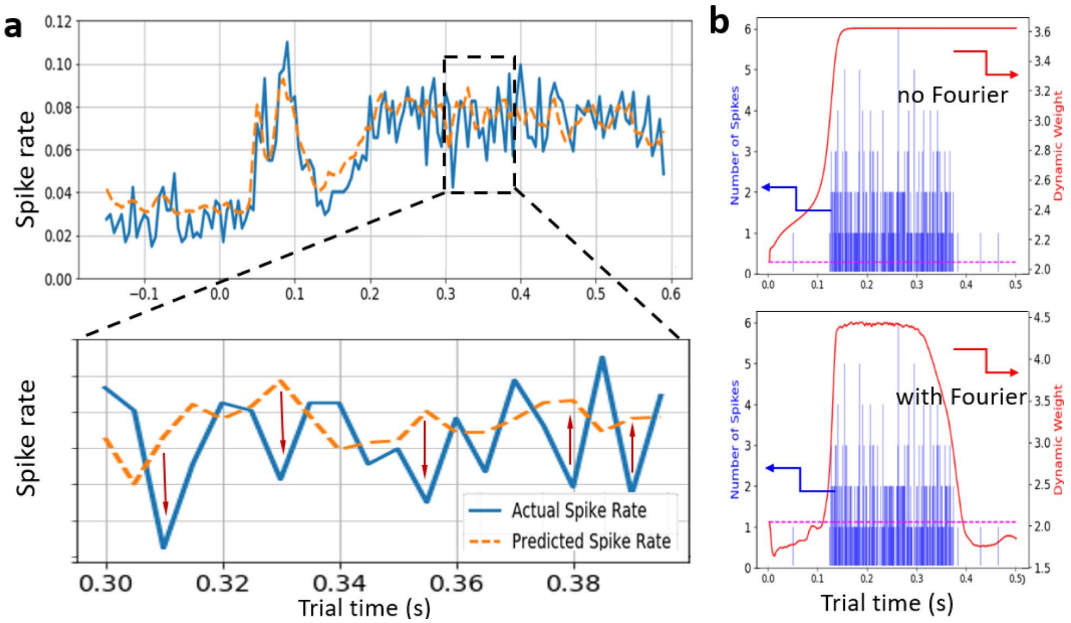

Fig.1 - figure supplement 1.

Model training and implementation

A) Loss optimization. Blue curve is actual spike rate for a representative unit taken from the VCN dataset (see below) as a function of trial time. The dotted yellow curve is a spike rate predicted by DyNetCP model during training. **Inset:** Loss function is designed to push the predicted spike rate to approach the actual spike rate during training. **B) Model performance with and without Fourier features.** Blue bars (left y-axis) represent a histogram of joint spiking probability (JPSTH anti-diagonal) for an example neuron pair with direct connection taken from the synthetic dataset (see below). Red curves (right y-axis) correspond to trial-averaged learned dynamic weights, while dotted magenta line represents static weight value. DyNetCP model without Fourier features (top plot) failed to properly localize the period where induced spiking is occurring, while use of Fourier features (bottom plot) enables to do so correctly.

learns static connectivity weights $w_{j\to i}^{d} \in \mathbb{R}^{M}$ that encode static network structure averaged over the time of the trial t, and $b_i \in \mathbb{R}$ are biases. We adopt a multivariate autoregressive GLM model[23] without temporal kernel smoothing that learns $\mathbf{W_{st}}$ as a function of a time lag d (**Fig.1B**). Sharp peak at short time lags implies increased probability of spiking of neuron j when neuron i is producing a spike that can be an indication that these two neurons are synaptically connected. An apparent time lag of the low-latency peak indicates a functional delay and defines the directionality of the putative connection. The static component of DyNetCP is implemented for all neurons jointly using a 1-dimensional convolution. Each convolutional filter contains the static weights used to predict the spiking probability for a single neuron as a function of the spiking history of all other neurons. The bias term b_i in Eq.2 is initialized to the logit function σ (i.e., inverse sigmoid) applied to the spike rate of each neuron calculated for a given time bin.

Dynamic connectivity inference

The dynamic component of DyNetCP (**Fig.1A**, right), i.e.,

$$E_{dyn}\left(x_i^t \middle| x^{t-M:t}, W_{off}\right) = \sum_{j\in e(i)} \sum_{d=1}^{M} w_{j\to i}^{d,t}\left(x_i^{1:t-1}, x_j^{1:t}\right) x_j^{t-d} \qquad \text{Eq.3}$$

learns the dynamic connectivity weights $w_{j\to i}^{d,t}$ which are a function of input spike trains $x_i^{1:t-1}$ and all other $x_j^{1:t}$. Each of these weights represents an offset to the time-averaged static weight at time t for a connection at time lag d (**Eq.2**). Hence, assuming the spikes of neuron i at a time lag d are influenced by spikes from all $x_j^{1:t}$, the total influence applied to the spiking of neuron i from neuron j at time t is $(w_{j\to i}^{d} + w_{j\to i}^{t,d}) x_j^{t-d}$. Unlike the static weights, these dynamic weights are allowed to change throughout an experimental trial as a function of the spiking history of the connected neurons.

The architecture of the dynamic part (**Fig.1C**) consists of several stages including generation of Fourier features, recurrent long-short-term-memory (LSTM) model, multilayer perceptron (MLP), embedding, and positional encoding. First, we shift each spike train such that each entry lies in {−1, 1} and then represent each spike train using Fourier features[40] that were recently introduced in the computer vision domain to facilitate the learning of high-frequency functions from low-dimensional input. Specifically, we encode every spike $x_j^i(t)$ using the following transformation:

$$\gamma\left(x_j^i(t)\right) = \left[\cos(2\pi b_1 x), \sin(2\pi b_1 x), \ldots, \cos(2\pi b_m x), \sin(2\pi b_m x)\right]^T \qquad \text{Eq.4}$$

Here, we use m = 64 features, where coefficients b_1, ..., b_m are linearly spaced between –1 and 1. We evaluate the use of Fourier features within the model on synthetic data consisting of a simulated network of neurons, where one neuron induces spiking in a second neuron during the middle 250 ms of each trial (**Fig.1 - figure supplement 1B**). DyNetCP without Fourier features is unable to properly localize the period where induced spiking is occurring, while the model with Fourier features can do so correctly.

The spike train features for each neuron are then input into separate LSTMs to produce an embedding per neuron per time step. Each of these LSTMs uses a separate set of weights and has a hidden dimension of 64. The LSTM embeddings are passed through two MLPs, f_{send} and f_{recv}, where f_{send} produces an embedding which represents the outgoing neural signal to other neurons and f_{recv} produces an embedding which represents the incoming signal from other neurons. Each of these MLPs consists of one linear layer with output size 64 and a ReLU activation. For each pair $n_j \to n_i$ of neurons being modeled, the send embedding $h_{s,j}(t)$ is concatenated with the receive embedding $h_{r,i}(t-1)$ as well as a time encoding $h_T(t)$ which represents the trial time and is represented as

$$h_{T(t)} = \begin{cases} sin\left(t/10000^{k/D_\tau}\right), k \text{ is even}, \\ cos\left(t/10000^{(k-1)/D_\tau}\right), k \text{ is odd}, \end{cases} \qquad \text{Eq.5}$$

where D_τ is the size of the positional encoding which we set to 128. Note that the send embedding contains spiking information through time t, i.e., it contains information about the most recent spikes, which is necessary to properly represent synchronous connections. Importantly, the receive embedding only contains spiking information through time $t - 1$ such that the output spiking probability is not trivially recoverable. Finally, this concatenated embedding is passed through a 2-layer MLP with hidden size 384 and a Rectified Linear Unit (ReLU) activation, producing the dynamic weight vector $w_{j\to i}^{t}(t)$ which contains dynamic weight offsets for each delay $d \in \{1, \ldots, M\}$.

Model training

The loss used to train the model consists of two terms. The first is a negative log likelihood over the predicted spike probabilities, which encourages the weights to accurately encode the influence of spiking from other neurons on the spiking of the neuron in question. The entire loss is written as

$$L(x;w) = \sum_{t=1}^{T}\sum_{j=1}^{N} x_j(t) log P\left(x_j(t) = 1 | x_j(t-M:t-1)\right) + \left(1 - x_j(t)\right) log\left(1 - P\left(x_j(t) = 1 | x_j(t - M \cdot t - 1)\right)\right) + \lambda ||\mathrm{w}||_2^2, \quad \text{Eq.6}$$

where w represents all the predicted static and dynamic weights, and λ is a coefficient used to balance the magnitudes of the losses. Loss optimization during training results in predicted spike rate (PSTH) that is approaching the actual spike rate (**Fig.1 – figure supplement 1A**).

We introduce a squared *L2* penalty on all the produced static and dynamic weights as the second term to discourage the network from overpredicting activity for times when no spikes are present $(x_j^{t-d} = 0)$ and the weight multiplied by zero is unconstrained. In these cases, adding the penalty provides a training target. For all experiments we used an *L2* weight between 0.1 and 1 that produced the best fit to the descriptive statistics results discussed in detail below (Methods).

Overall, once the architecture of **Fig.1C** is established, there are just a few parameters to optimize including L*2* regularization and loss λ coefficient. Other variables, common for all statistical approaches, include bin sizes in the lag time and in the trial time. Decreasing the bin size will improve time resolution while decreasing the number of spikes in each bin for reliable inference. Therefore, the number of spikes threshold and other related thresholds need to be adjusted as discussed in detail in the Methods, Section 4.

Results

The DyNetCP model is designed to be trained in a single step to produce both static and dynamic weight matrices simultaneously for the whole dataset. However, for the purpose of this work, we are interested in verification and detailed comparative analysis of the model performance that enables clear justification for the choice of model parameters. Therefore, here, training of the model to analyze a new dataset is implemented in two separate stages. In the first stage, only the static weights $\mathbf{W_{st}}$ are trained for all the valid neurons while the dynamic weights $\mathbf{W_{dyn}}$ are all set to zero. In the second stage, the static model parameters and static weights are fixed, and we train only the dynamic component of the model.

This two-stage architecture enables detailed comparison of static and dynamic matrices to classical descriptive statistical methods as well as to modern probabilistic models. In the virtual absence of synthetic or experimental datasets with known GT such comparisons are becoming crucial for tuning the model parameters and for validation of the results. It is especially important for validation of the dynamic stage of the DyNetCP since it predicts $\mathbf{W_{dyn}}$ that describes temporal variation of the connection strength that is assigned to individual neurons, and, therefore, could

not be directly compared to most of the population dynamics models that produce temporal trajectories in a latent feature space of the whole population[26–29]. In what follows we consider these comparisons separately.

Static DyNetCP can faithfully reproduce descriptive statistics cross-correlogram

The DyNetCP formulation of its static stage (Eq.2) is similar to classical cross-correlogram[15,30] (CCG) between a pair of neurons n_1 and n_2 that is defined as:

$$\mathrm{CCG}(\tau) = \frac{1}{M}\sum_{i=1}^{M}\frac{\sum_{t=1}^{T} x_1^t(i)x_2^{t+\tau}(i)}{\theta(\tau)\sqrt{\lambda_1\lambda_2}}, \qquad \text{Eq.7}$$

where τ represents the time lag between spikes from n_1 and n_2, λ_j is the spike rate of neuron j, and $\theta(\tau)$ is a triangular function which corrects for the varying number of overlapping bins per delay. However, instead of constructing the statistical CCG histogram for each pair individually, the model given in Eq.2 infers coupling terms from spiking history of all N neurons jointly. Typically, to minimize the influence of a potential stimulus-locked joint variation in population spiking that often occurs due to common input from many shared presynaptic neurons, a jitter correction[15,30,41–43] is applied. To directly compare the results of static DyNetCP with jitter-corrected CCG, we train two static models (Methods) – one on original spike trains and the second on a jitter-corrected version of the data generated using a pattern jitter algorithm[41] with a jitter window of 25ms.

For this comparison we used a subset of the Allen Brain Observatory-Visual Coding Neuropixels (VCN) database[15] that contains spiking activity collected in-vivo from 6 different visual cortical areas in 26 mice (Methods, **Table 1**) passively viewing a “drifting grating” video (top left inset in **Fig.1A**). For a pair of local units (spatially close units from Layer 5 of the VISam area) comparison of static DyNetCP (**Fig.2A**, red curve) with jitter-corrected CCG (**Fig.2A**, black curve) shows close correspondence (Pearson correlation coefficient r_p=0.99 and p-value P_p<0.0001). Residual analysis (**Fig.2A**, bottom panel) shows a mean value of 0.01±0.02 SEM (**Fig.2A**, top right panel) that is smaller than the CCG values on the flanks (bottom right panel) (mean:0.11±0.06 SEM). For such a local connection the peak is narrow (~2ms) with a functional delay of −2.3ms. For a pair of spatially distant units (units in VISam and VISp areas) a comparison of static DyNetCP (**Fig.2B**, red curve) with jitter-corrected CCG (**Fig.2B**, black curve) also shows close correspondence (r_p=0.99 and P_p<0.0001). For such a distant connection the peak is wider (~9ms) with a functional delay of −5.8ms. Further examples of comparisons of both models for all the units in the session showed similar results (see accompanying Jupyter Notebook).

Following the common formulation, a putative excitatory (or inhibitory) synaptic connection can be considered statistically significant for both methods when the magnitude of the short-latency peak (or trough) exceeds the peak height threshold α_w (lower than $-\alpha_w$) compared to the standard deviation (SD) of the noise in the flanks far from the peak[15,19,25,30] (whisker plots on top right panels in **Fig.2A,B**).

Static DyNetCP reproduces GT connections on par with alternative probabilistic method

We compare the performance of DyNetCP to a recent GLM-based cross correlation method (GLMCC)[25] that detects connectivity by fitting a parameterized synaptic potential filter (**Fig.2C**, magenta). For these experiments, we use the synthetic dataset[25] consisting of 1000 Hodgkin-Huxley (HH) neurons with known GT synaptic connections (Methods). We focus specifically on recovering ground-truth (GT) excitatory connections. The $\mathbf{W_{st}}$ inferred by DyNetCP for a representative pair of neurons (**Fig.2C**, red) reproduces well the short-latency narrow peak and the flanks of the postsynaptic potential (PSP) filter learned by GLMCC (**Fig.2C**,

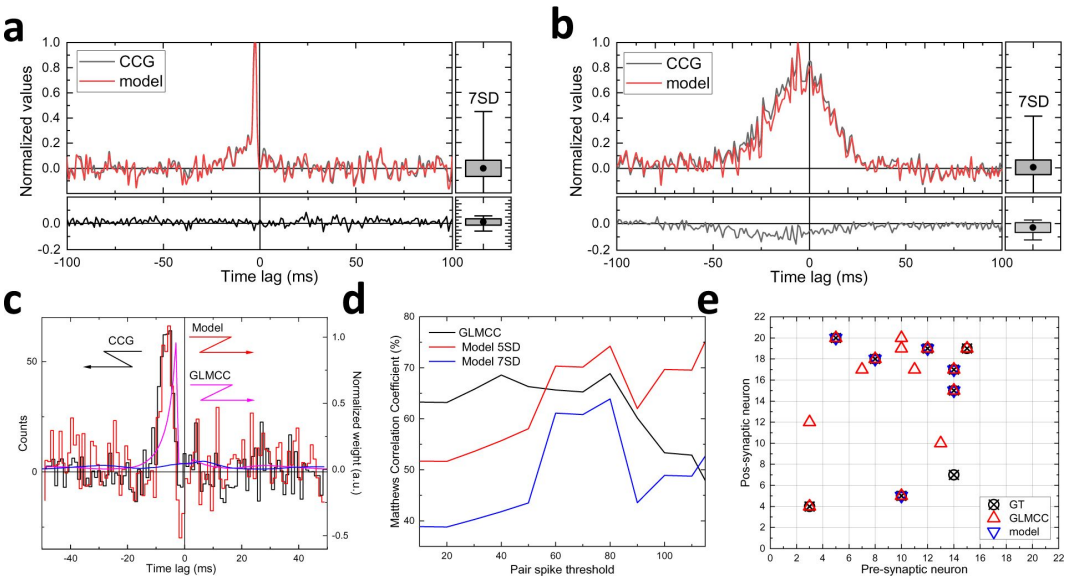

Figure 2.

Comparison of inferred static connectivity to alternative methods.

A) Comparison of static DyNetCP (red curve) with jitter-corrected CCG (black curve) for a representative pair of local units (session 771160300, spatially close units from Layer 5 of the VISam area). Residuals (bottom panel) and residual analysis (right panels). **B)** Comparison of static DyNetCP (red curve) with jitter-corrected CCG (black curve) for a representative pair of spatially distant units (session 771160300, units from VISam and VISp areas). **C)** Comparison of jitter-corrected CCG (black), GLMCC (magenta), and DyNetCP (red) weights for a pair of excitatory HH neurons from a synthetic dataset. **D)** MCC calculated for GLMCC (black) and for DyNetCP with α_w =5SD (red) and 7SD (blue). **E)** Static connectivity $\mathbf{W_{st}}$ for a subset of excitatory HH neurons with GT (crossed circles) compared to connections recovered by GLMCC (red triangles) and DyNetCP (blue triangles).

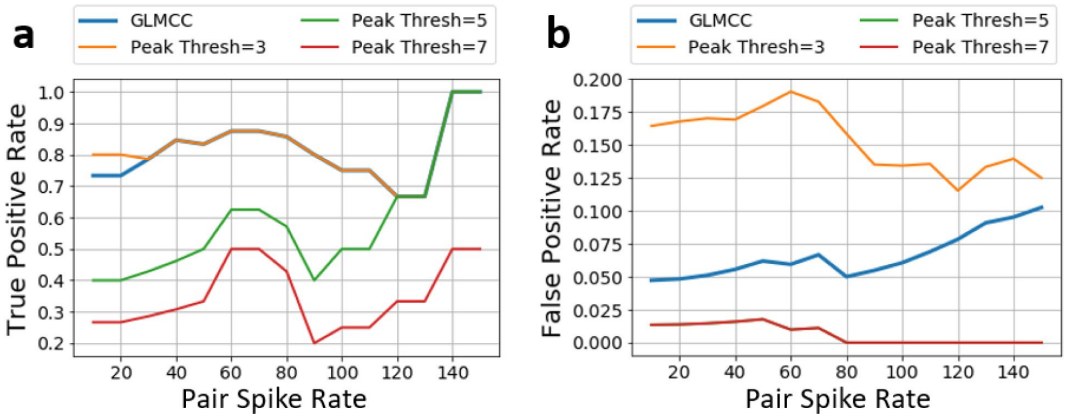

Fig.2 - figure supplement 1.

TP and FP rates as a function of pair spike threshold

A) Recovery of True Positive (TP) connections in HH synthetic dataset. TP connections recovered by DyNetCP model at different pair spike thresholds α_p. Yellow, green, and red curves correspond to peak threshold taken as 3SD, 5SD, and 7SD, respectively. TP connections recovered by GLMCC model are shown by blue curve. Since a predicted connection is counted as a *TP* only once (i.e., $i \rightarrow j$ and $j \rightarrow i$ do not count as two negatives if *i* is not connected to *j*) and the number of *GT* connections decreases when α_p increases, the MCC exhibits an increase beyond α_p=100. **B) Generation of False Positive (TP) connections in HH synthetic dataset.** FP connections generated by the DyNetCP model at different pair spike rates. Yellow, green, and red curves correspond to peak threshold α_p taken as 3SD, 5SD, and 7SD, respectively. FP connections recovered by GLMCC model are shown by blue curve.

Session	Units	Clean units	Valid Units	Valid Units %	Valid Pairs	Run	Run %
766640955	842	145	25	17%	24	50	10%
767871931	713	185	53	29%	49	146	30%
768515987	802	198	41	21%	43	4	1%
771160300	930	223	35	16%	35	115	24%
771990200	546	108	42	39%	41	43	9%
774875821	649	172	43	25%	12	126	26%
778240327	784	275	78	28%	56	413	86%
778998620	793	233	44	19%	15	240	50%
779839471	863	203	29	14%	17	4	1%
781842082	833	229	36	16%	38	66	14%
786091066	700	306	17	6%	13	408	85%
787025148	696	134	18	13%	21	110	23%
789848216	415	81	31	38%	26	183	38%
793224716	781	198	82	41%	77	171	36%
794812542	1005	348	38	11%	30	54	11%
816200189	634	161	46	29%	75	11	2%
819186360	531	166	26	16%	13	13	3%
819701982	585	163	38	23%	29	440	92%
821695405	474	148	38	26%	28	40	8%
829720705	529	232	54	23%	43	88	18%
831882777	657	264	65	25%	62	391	81%
835479236	582	199	36	18%	38	70	15%
839068429	742	150	49	33%	57	401	84%
839557629	450	136	26	19%	11	307	64%
840012044	758	179	67	37%	97	135	28%
847657808	874	231	53	23%	70	72	15%
Total	18168	5067	1110	23%	1020	4101	33%

Table. 1.

Experimental dataset recorded in-vivo in 6 visual cortices.

Sessions used for model training and analysis taken from the publicly available Allen Brain Observatory-Visual Coding Neuropixels (VCN) database. We use a "functional connectivity" subset of these recordings corresponding to the "drifting grating 5 repeats" setting recorded for animals. Filtering of recorded units (see statistical analysis criteria below) and classification of valid pairs results in a significant reduction of units (5.6% of raw units or 23% of clean units) used for dynamic connectivity inference. The last two columns represent the number and percentage of trials when the animal was running with average speed over 5cm/sec

magenta). Comparing to CCG histogram (**Fig.2C**, black), the DyNEtCP is performing much better than GLMCC (r_p=0.67 and P_p<0.001), however the results are not as directly interpretable as GLMCC that outputs synaptic weight from the PSP fitting. Both models, however, can infer presence or absence of the connection by examining the height of the low latency peak.

To facilitate a performance comparison, we use the Matthews Correlation Coefficient (MCC), defined as

$$\mathrm{MCC} = \frac{TP \times TN - FP \times FN}{\sqrt{(TP+FP)(TP+FN)(TN+FP)(TN+FN)}}, \qquad \text{Eq.8}$$

where *TP*, *TN*, *FP*, and *FN* are true positive, true negative, false positive, and false negative pair predictions, respectively. MCC optimization balances between maximizing the number of *TP* pairs recovered while minimizing the number of *FP* pairs which are predicted.

Performance of all three methods, classical CCG and probabilistic GLMCC and DyNetCP, will be strongly affected by the total number of spikes available for inference. To ensure the statistical significance of connections inferred by all 3 methods a large enough number of spikes should be present in each time bin (Methods) that is tracked by two threshold parameters: a unit average spike rate α_s, and a pair spike parameter α_p that is the number of spikes that both units generate in a time window of interest (Methods). **Fig.2D** compares the performance of DyNetCP and GLMCC on a synthetic dataset, while the number of spikes present for learning is varied via a threshold pair spike parameter α_p. Increasing α_p ensures statistically significant inference about the presence or absence of a connection[25] (Methods). As α_p increases, the MCC for both models shows a maximum around α_p=80 corresponding to the optimal balance. For a conservative value of α_w=7SD (blue), the MCC for the DyNetCP model is 63%, approaching the performance of GLMCC (68%, black). When α_w is relaxed to 5SD (red), DyNetCP recovers a larger number of TP with a reasonable increase of FP connections (**Fig.2 - figure supplement 1**), increasing MCC up to 74%, thus outperforming GLMCC. Overall, as long as DyNetCP has access to a sufficient number of spikes for inference, it can restore GT static connectivity on par with or even better than GLMCC (**Fig.2E**).

Though GLMCC performs well in recovering static network structure and it produces directly biologically interpretable results, we emphasize that GLMCC is not compatible with modeling the network dynamics and thus cannot be integrated into DyNetCP. Specifically, our goal is to model the correlations of spiking of a network of neurons and track the changes of these correlations across time. GLMCC learns correlations as a function of the time lag relative to the spiking time of a reference neuron. It is hence unable to link correlations to specific moments in a trial time. Therefore, it cannot represent the dynamics of correlations, preventing its use in analysis of network activity relative to subject behavior. In contrast, the formulation of static DyNetCP model of Eq.2 provides a weight matrix $\mathbf{W_{st}}$ which is compatible with the subsequent inference of time-dependent dynamic weights $\mathbf{W_{dyn}}$.

Static connectivity inferred by the DyNetCP from in-vivo recordings is biologically interpretable

Recent reconstruction of the brain-wide connectome of the adult mouse brain using viral tracing of axonal projections[4,5] enables assignment of anatomical hierarchical score values to cortico-cortical projections across visual cortices[4] (**Fig.3A**). Similarly, measuring the time lags of the maximum peaks in the CCG of recorded neuron pairs (e.g. as in **Fig.1B**) can be used to assess a hierarchy of functional connectivity between different cortical areas. Such analysis of functional delays extracted from massive recording of spiking activity across visual cortices[15] revealed strong correlation of area-averaged functional delays and the hierarchical score values indicative of the hierarchical processing of visual information. Classical CCG (as well as GLMCC), however, recovers static network structure by modeling pairwise correlations and hence must be run

separately for each pair in the dataset without considering the relative influence of other pairs in the network. Each neuron, however, is connected to thousands of others and is potentially contributing to multiple networks simultaneously. In contrast, DyNetCP learns connections of an entire network jointly in one pass and can track multiple connections beyond pair-wise. It is, therefore, instructional to compare the hierarchical interactions between visual cortices inferred by DyNetCP to CCG results using the same large-scale in-vivo VCN dataset[15]. Following the previous methodology[15,19], functional delays corresponding to the time lags of jitter-corrected CCG peaks are determined for all recorded pairs across all six cortical areas with peak amplitudes above α_w of 7SD (5023 pairs, n=26 animals). The median time lags averaged across pairs within a given visual area (**Fig.3B**) are identified as the area's functional delay. When plotted against the hierarchical score difference (**Fig.3C**, red triangles), the area median functional delays exhibit strong correlation (r_p=0.76 and P_p<0.0001).

The DyNetCP trained on the same 5023 pairs with $\mathbf{W_{st}}$ peak amplitudes above α_w of 7SD, whose shape is statistically indistinguishable (typical r_p>0.9 and P_p<0.0001) from the corresponding jitter-corrected CCG, produce similar functional delays (**Fig.3D**). The median functional delays predicted by DyNetCP by learning from all units (**Fig.3C**, blue triangles) also show strong correlation (r_p=0.73, P_p<0.0001) with the visual area anatomical hierarchical score difference[5], very closely replicating (r_p=0.99, P_p<0.0001) the correlation observed with the descriptive pairwise CCG-based analysis. Therefore, the static DyNetCP is able to confirm previous observation of hierarchical organization of inter-area functional delays[15].

Comparison of inferred dynamic connectivity to descriptive statistical methods

Once the static connectivity $\mathbf{W_{st}}$ is established and verified, the dynamic stage of DyNetCP learns $\mathbf{W_{dyn}}$ that is strongly temporally modulated (**Video 1**). While no GT data are currently available to verify the model performance, model predictions can be compared to a classical pairwise Joint Peristimulus Time Histogram[39] (JPSTH) that represents the joint correlations of spiking between two neurons and their variation across time. Specifically, given trial-aligned data with a trial length of T bins, the JPSTH is a $T \times T$ matrix where each entry (a, b) represents the percent of trials where neuron i spiked at time a and neuron j spiked at time b. For an example pair of excitatory spatially close units located in Layer 5 of the VISp area (session 766640955) corresponding JPSTH is shown in **Fig.4A**. Averaging over the columns of the JPSTH recovers the peristimulus time histogram (PSTH) of neuron i (left panel in **Fig.3A**), while averaging over the rows of the JPSTH recovers the PSTH for neuron j (bottom panel in **Fig.3A**). Since DyNetCP learns the conditional probability of the spiking of one neuron conditioned on others, we cannot directly compare dynamic weights to a standard JPSTH, which models joint correlations. Instead, for a proper comparison, we use a conditional joint peristimulus time histogram (cJPSTH), where we divide the columns of the JPSTH by the PSTH of neuron i (**Fig.4B**). This changes the meaning of each entry (a, b) in the cJPSTH that represents the conditional probability that neuron j spikes at time b, conditioned on neuron i having spiked at time a (**Fig.4C**).

The dynamic weights $\mathbf{W_{dyn}}$ matrix inferred by DyNetCP for the same example pair (**Fig.4D**, see also (**Video 1**) reveal strong temporal modulation peaking at around 70ms, 220ms, 300ms, and 480ms indicating increased connection strength. Comparison with the cJPSTH matrix (**Fig.4E**) shows similar temporal variation. This comparison can be used to validate the choice of an optimal squared $L2$ penalty that is introduced into the model loss function (Eq.6) to compensate the sparseness and irregularity of spiking often observed in cortical recordings (Methods). For a given set of thresholds α_w, α_s, and α_p, scanning of $L2$ from 0.01 to 10 (**Fig.4 – figure supplement 1A**) demonstrates statistically significant correlation (r_p>0.77 and P_p<0.001) of the dynamic weights $\mathbf{W_{dyn}}$ matrices and cJPSTH matrices observed for all $L2$ values with the best results obtained for $L2$ between 0.1 and 1 (**Fig.4 – figure supplement 1B**). The two-sided paired equivalence test (TOST) (Fig.3 – figure supplement 1C) confirms that the average difference

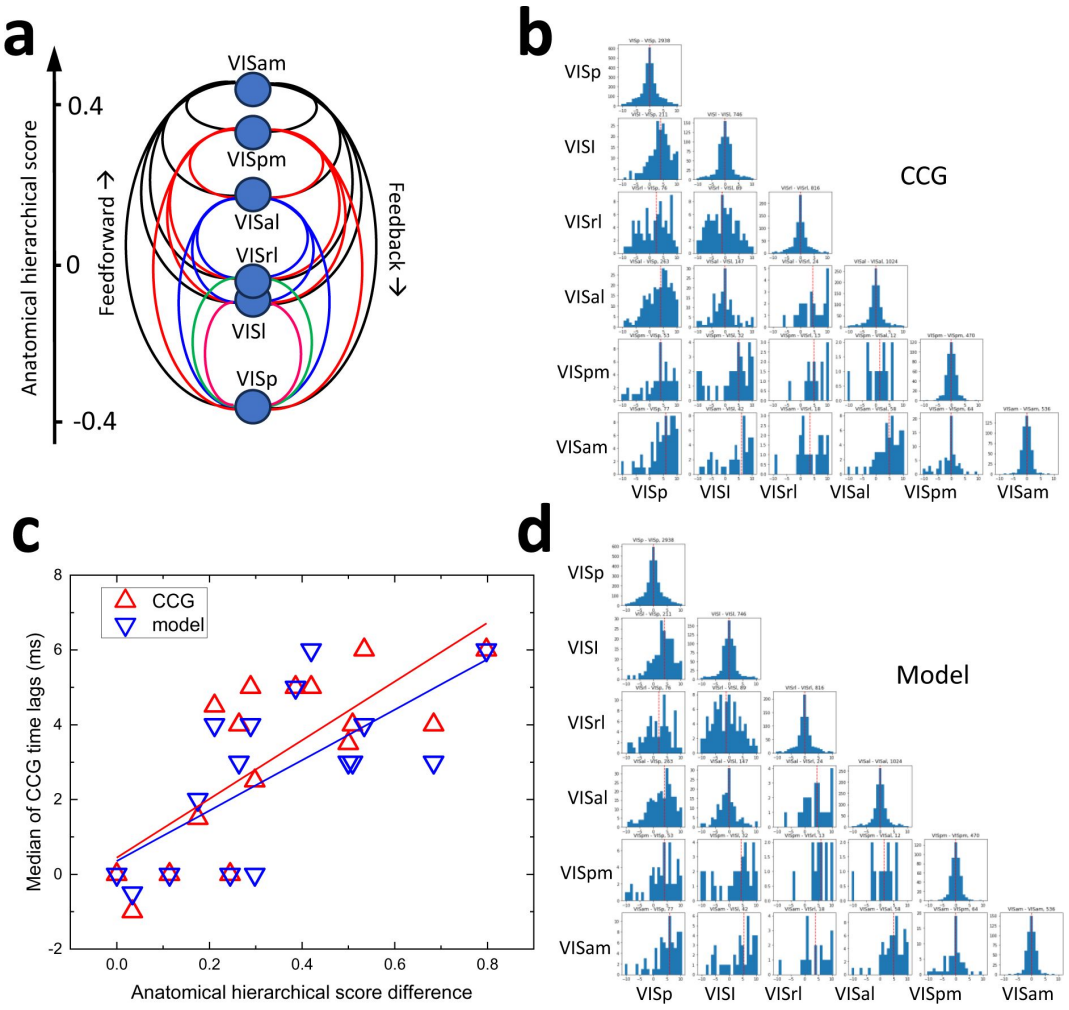

Figure 3.

Static connectivity inferred by the model is biologically interpretable.

A) Feedforward and feedback connections between 6 cortical areas ordered with respect to their anatomical hierarchy scores (after Ref.4). **B)** Histograms of the functional delays extracted from the jitter-corrected CCG for all pairs across all 26 sessions for each visual area combination. Dashed red line indicates the median of the distribution. **C)** Comparison of median functional delays vs anatomical hierarchy score difference extracted by DyNetCP (blue triangles) and by jitter-corrected CCG (red triangles) (VCN dataset, n=26 animals). **D)** Histograms of the functional delays inferred by static DyNetCP across all 26 sessions of VCN dataset for each visual area combination. Dashed red line indicates the median of the distribution.

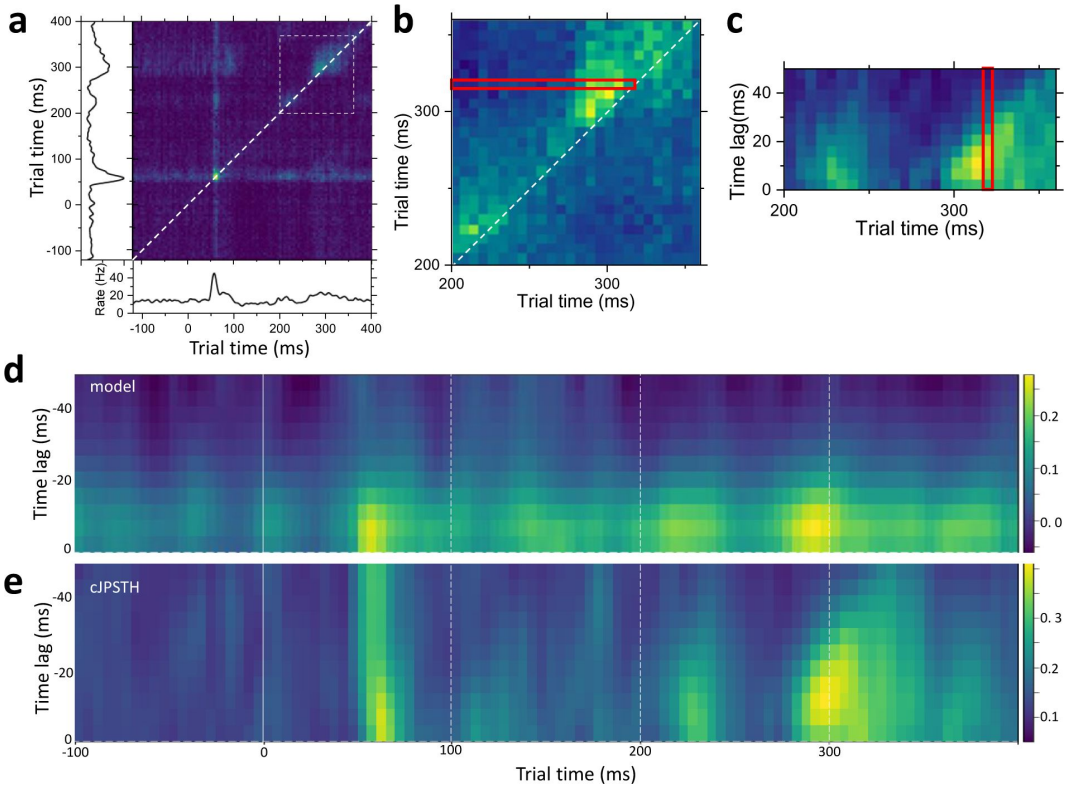

Figure 4.

Comparison of inferred dynamic connectivity to descriptive statistical methods.

A) An example of JPSTH for a local pair of excitatory units (session 766640955 of the VCN dataset, spatially close units from Layer 5 of the VISp area). Panels on the left and at the bottom show corresponding spike rates for receive and send units, correspondingly. White dotted square corresponds to the area of interest. See also **Video 1**. **B)** Construction of the conditional cJPSTH. Pixels from the white dotted square in A) are normalized by spiking rate of the send neuron. Row of pixels marked by red rectangle is used in C). **C)** cJPSTH corresponding to the white dotted square in A). Red rectangle corresponds to red rectangle pixels in B). **D)** Dynamic weight $\mathbf{W_{dyn}}$ for the same pair of excitatory units inferred for *L2* of 1 (see also **Video 1**). **E)** cJPSTH for the same pair of units.

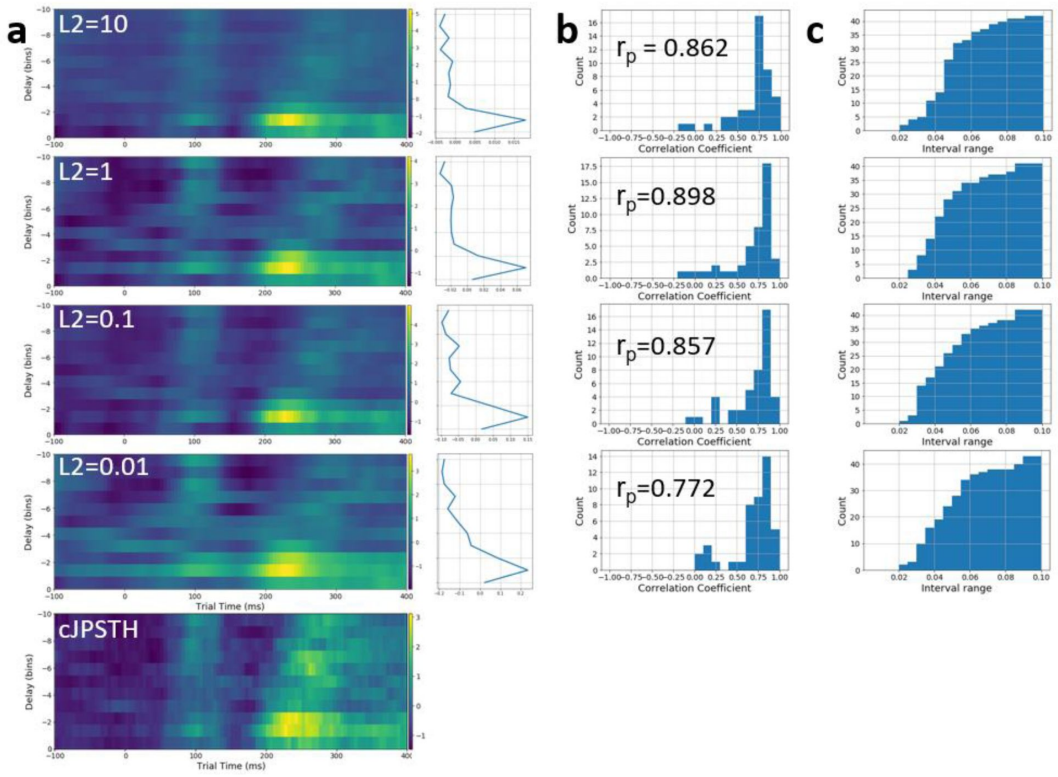

Fig.4 – figure supplement 1.

Tuning loss parameter.

A) Set of dynamic weights $\mathbf{W_{dyn}}$ for a local pair of excitatory VISp neurons (session 771160300, same as in **Fig.4D,E**) learnt with different *L2* values. The corresponding cJPSTH is shown on the bottom. Left column shows a set of corresponding static weights $\mathbf{W_{st}}$. **B)** A histogram of Pearson correlation coefficients between the dynamic weights and cJPSTH for each pair (comparing each pixel of the weight/cJPSTH matrix) calculated for all 41 pairs found to be significant for this session. **C)** The two-sided paired equivalence tests (TOST) for all 41 pairs in this session indicate that the average difference between normalized weights inferred from both models is smaller than 0.09.

between normalized weights inferred from both models is smaller than 0.09. Therefore, the DyNetCP reliably recovers the time-dependent dynamic weights $\mathbf{W_{dyn}}$ even in the presence of strong nonstationary spiking irregularities and sparse spiking.

Model enables discovery of cellular-level dynamic connectivity patterns in visual cortex

The model architecture (**Fig.1A**) designed with two interacting static and dynamic parts enables justification of the choice of model parameters and verification of model inference results by comparison with the results of descriptive statistical methods. Therefore, even in the absence of experimental or synthetic datasets with known ground truth (GT) of cellular-level dynamic connectivity, the model can provide an otherwise unattainable insights into dynamic flows of information in cortical networks. To ensure statistical significance of inferred connections three thresholds (Methods) were applied simultaneously to each of the 26 sessions in the VCN database: a unit average spike rate α_s>1Hz, a pair spike rate threshold α_p>4800, and a static weight peak threshold α_w>7SD that produced 808 valid units forming 1020 valid pairs across all 6 cortical areas (Methods, **Table 1**).

Reconstruction of dynamic connectivity in a local circuit

To illustrate reconstruction of static and dynamic connectivity in a local circuit we use recording from a single animal (session 819701982) from a single Neuropixel probe implanted in the VISam area. Application of three thresholds α_s, α_p, and α_w to all clean units passing quality metrics (Methods) produce 6 pairs with statistically significant (α_w>7SD) and narrow (<2ms) peak in a static weight $\mathbf{W_{st}}$ (Methods, **Table 2**) indicating strong putative connections (**Fig.5A**). Units are classified as excitatory (waveform duration longer than 0.4ms) or inhibitory (less than 0.4ms) and are assigned to cortical depth and cortical layers based on their spatial coordinates (Methods). Directionality of the connection is defined by negative functional time lag in a static weight $\mathbf{W_{st}}$ (or jitter corrected CCG) binned at 1ms. Local circuit reconstructed from static weights matrices is shown in **Fig.5B**. Corresponding dynamic matrices $\mathbf{W_{dyn}}$ (**Fig.5C**) for the same pairs demonstrate strong temporal modulation (see also **Video 2**). Prior to presentation of a stimulus (t<0ms) the inhibitory drives (negative values of $\mathbf{W_{dyn}}$ marked by deep blue color in **Fig.5C**) prevail. The first positive peak of $\mathbf{W_{dyn}}$ around 70ms (positive values of $\mathbf{W_{dyn}}$ marked by bright yellow color in **Fig.5C**) is shared by all but one pair. Such synchronous spiking at short time lags does not necessarily indicate a TP direct connection but can also be an FP artefact induced by arrival of afferent signals[44]. However, at later times, additional strong peaks appear for some of the pairs that are not accompanied by corresponding increase of the firing rates. Some of the pairs form an indirect serial chain connections (e.g., 3→2 and 2→4 **Fig.5B**) that can also generate confounding FP correlations that is notoriously difficult to identify using descriptive statistical models[24]. However, the DyNetCP being a probabilistic model might lessen the impact of both the common input and the serial chain FP artefacts by abstracting out such co-variates that do not contribute significantly to a prediction. For example, the $\mathbf{W_{dyn}}$ for a potential 3→4 artefactual connection does not show peaks expected from the serial chain.

To aid identification of such confounding FP connections, we performed preliminary tests on a synthetic dataset that contain a number of common input and serial chain triplets and were able to identify them by comparing $\mathbf{W_{dyn}}$ values at a given trial time to corresponding $\mathbf{W_{st}}$ (Methods). **Figure 6** shows temporal evolution of normalized dynamic weight values taken from **Fig.5C** along the trial time axis at corresponding functional time lags. We assign excitatory (inhibitory) connection to a given pair as present when the ratio $\mathbf{W_{dyn}}/\mathbf{W_{st}}$ is larger (or smaller) than 1 (−1). Corresponding dynamic graphs for a local circuit of **Fig.5** are shown in **Fig.6B** for characteristic trial times. Such dynamic circuit reconstruction is aided by observation of the troughs (inhibitory connection) and peaks (excitatory connection) in the $\mathbf{W_{dyn}}$ cross-sections along the lag time axis taken at a given trial time (**Fig.6 – figure supplement 1**, see also **Video 2**).

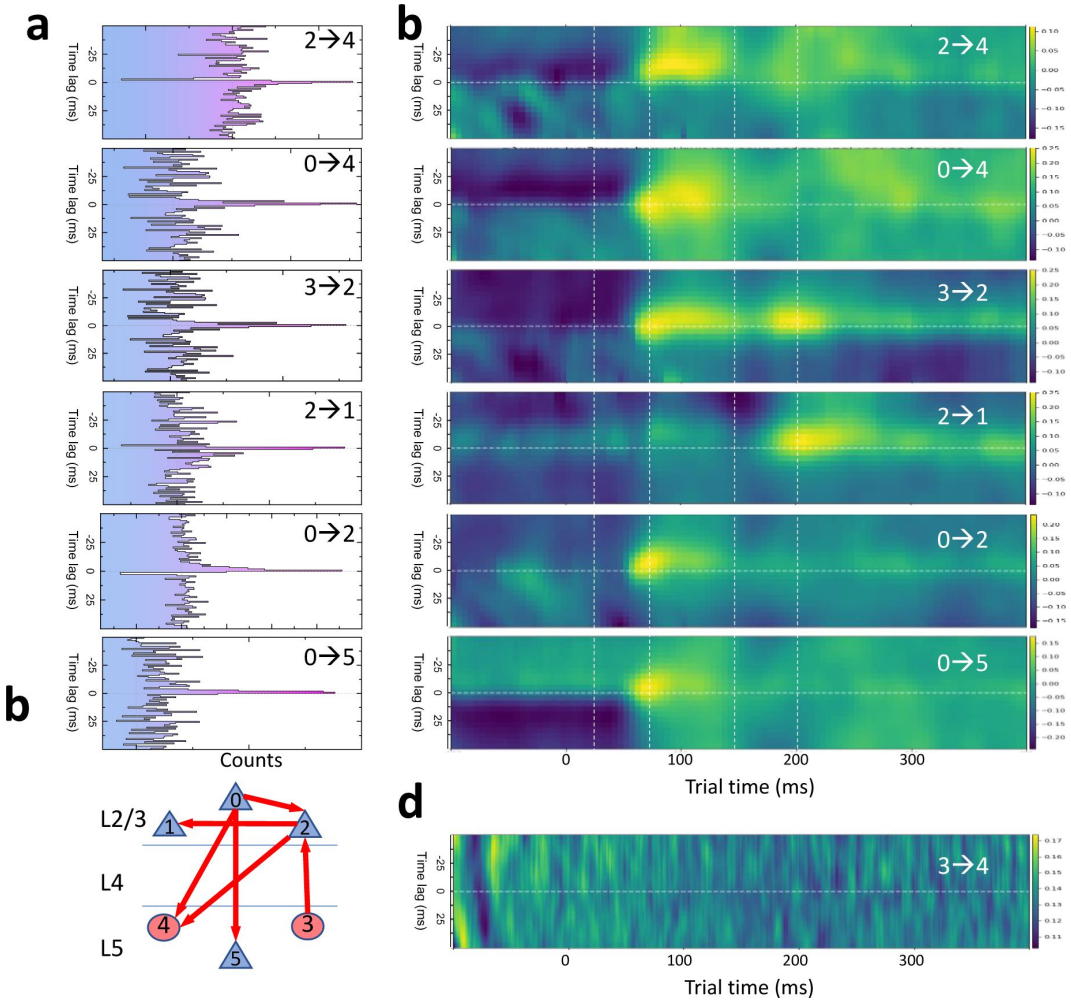

Figure 5.

Model enables discovery of cellular-level dynamic connectivity patterns in visual cortex.

A) Jitter-corrected static weights $\mathbf{W_{st}}$ for a connected pairs in an example local circuit (session # 819701982, VISam area). Units are numbered by local indices (Methods, **Table 2**). **B)** Dynamic weights $\mathbf{W_{dyn}}$ for the same pairs. **C)** Schematic diagram of static directional connectivity in pairs in a local circuit in A). Circles and triangles correspond to excitatory and inhibitory units, respectively. **D)** An example of a dynamic weight $\mathbf{W_{dyn}}$ for a pair (3→4) classified as un-connected.

parameter	valid pairs					
send_local_id	2	0	3	2	0	0
send_unit_id	951137428	951137567	951137152	951137428	951137567	951137567
send_rate (Hz)	8.35	29.92	15.05	8.35	29.92	29.92
send_waveform (ms)	0.30	0.25	0.59	0.30	0.25	0.25
send_ecephys_channel_id	850297842	850297858	850297816	850297842	850297858	850297858
send_probe_vertical_position	3180	3260	3060	3180	3260	3260
send_layer	3	3	5	3	3	3
recv_local_id	4	4	2	1	2	5
recv_unit_id	951137059	951137059	951137428	951137446	951137428	951136981
recv_rate (Hz)	18.00	18.00	8.35	14.04	8.354601718	40.75
recv_waveform (ms)	0.58	0.58	0.30	0.23	0.302177554	0.22
recv_ecephys_channel_id	850297810	850297810	850297842	850297844	850297842	850297796
recv_probe_vertical_position	3020	3020	3180	3200	3180	2960
recv_layer	5	5	3	3	3	5
send_recv_distance (μm)	160	240	-120	-20	80	300
max_static_weight	0.08	0.12	0.18	0.17	0.19	0.13
max_dynamic_weight	0.21	0.22	0.60	0.50	0.41	0.39

Table. 2.

Experimental dataset used for reconstruction of local circuit in Fig.5 and Fig.6

Clean units (passed unit quality metrics) that from valid pairs (passed through all three thresholds α_s, α_p, and α_w) from recordings in VISam area in session 819701982. Units are classified as excitatory (waveform duration longer than 0.4ms) or inhibitory (less than 0.4ms) and are assigned to cortical depth and cortical layers based on their spatial coordinates. Local circuit reconstructed from static weights matrices (max_static weight) is shown in **Fig.5B**. Maximum dynamic weight (max_dynamic_weight) is taken at functional time lag. Distance between units (send_recv_distance) is estimated from vertical positions of corresponding principal electrodes (probe_vertical_position).

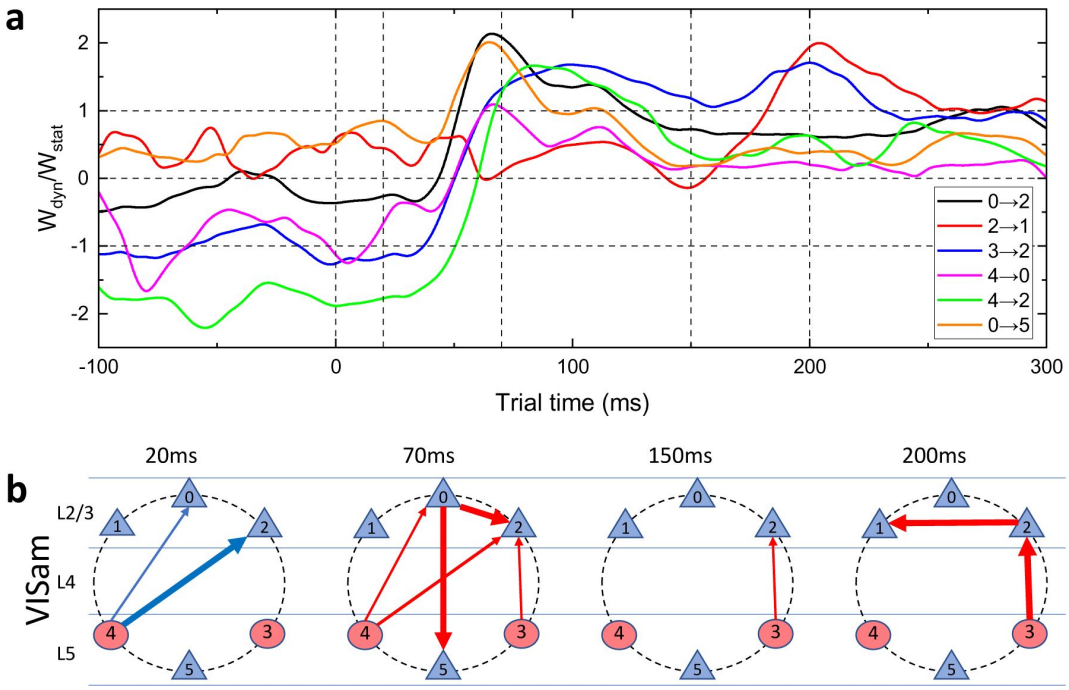

Fig. 6.

Temporal variation of dynamic weight and reconstruction of dynamic local circuit.

A) Normalized dynamic weights for all valid pairs in an example local circuit (session # 819701982, VISam area). Units are numbered by local indices. **B)** Schematic diagram of dynamic connectivity in a local circuit for different trial times. Circles and triangles correspond to excitatory and inhibitory units, respectively. The size of blue (red) arrows reflects the dynamic weight of the inhibitory (excitatory) connection at a given time.

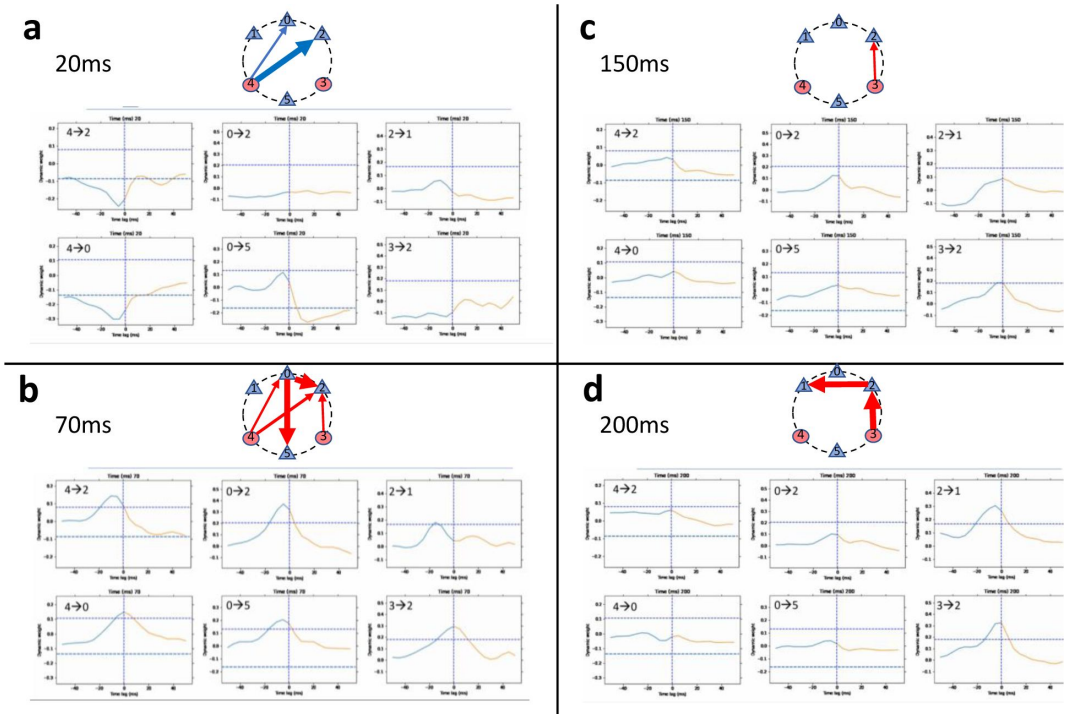

Figure 6 - figure supplement 1.

Reconstruction of a dynamic connectivity in a local circuit.

Dynamic weights $\mathbf{W_{dyn}}$ for 6 valid pairs in an example local circuit in **Fig.6** taken at different trial times. **A)** at 20ms. **B)** at 70ms. **C)** at 150ms. **D)** at 200ms. Reconstruction of dynamic connectivity is shown on top of each figure. Circles and triangles correspond to excitatory and inhibitory units, respectively. The size of blue (red) arrows reflects the dynamic weight of the inhibitory (excitatory) connection at a given time. See also **Video 2**.

Note, that since DyNetCP, as opposed to population dynamic models[26–29], learns latent variables assigned to individual units, the anatomical and cell-type specific information in static graph of **Fig.5B** is preserved. As in **Fig.5B**, units in the circuit of **Fig.6B** are ordered with respect to their cortical depth, assigned to specific cortical layers, classified as inhibitory (excitatory) based on their waveform duration. Further analysis of optotagging[45] (Methods) was used to identify that none of inhibitory units in this local circuit belong to a Vasoactive Intestinal Polypeptide (Vip) cell class. DyNetCP can also be trained separately on trials when animal was running, and animal was at rest (Methods, **Table 1**) to explore the role of brain state on dynamic connectivity patterns. Therefore, not only DyNetCP can provide static connections in this local circuit, but, more importantly, can also track the time epochs when individual cellular-level connections are activated or inhibited that are time-aligned to the stimulus presentation, brain state, and behavior.

Dynamic connectivity in VISp primary visual area

Going beyond local circuits, the dynamic analysis of information flows during stimulus presentation can be extended to area-wide dynamic maps. However, with the aggressive choice of threshold parameters (α_s>1Hz, α_p>4800, α_w>7SD) the average number of valid pairs per session (Methods, **Table 1**) is relatively low to generalize (mean:39 ± 4 SEM). To analyze area-wide connectivity, an example of cellular-level dynamic interactions in primary visual area VISp learned from all 26 sessions is shown in **Video 3**. Still frames from this video are presented in **Fig.7A** for a number of characteristic trial times. Units are ordered by cortical depth and assigned to cortical layers. Circles represent the magnitude of a dynamic weight $\mathbf{W_{dyn}}$ taken at corresponding functional time lag. The circles diameter is proportional to the dynamic offset $\mathbf{W_{dyn}} - \mathbf{W_{st}}$. The dynamic weights are changing over the time of the trial (**Video 3**) and exhibit interactions between excitatory cells (red circles), inhibitory cells (blue circles) and mixed drives (magenta circles). While excitatory-excitatory connections are mostly activated within layer 4 and layer 5, connections involving inhibitory cells dominate inter-layer interactions between all the layers. Feedforward extra-laminar interactions (e.g., input layer 4 is driving supergranular layer 2/3 and infragranular deep layers 5 and 6) reveal formation of neuronal ensembles across all the cortical depth. Feedback interactions are also distributed across the cortical depth with nearly the same maximum weights. These observations are inconsistent with static connection efficacy extracted from CCG peaks recorded in V1 columns in anesthetized monkeys[46] that indicate the efficacy greatly diminished within <200μm from the source. It is consistent, however, with static spike transmission strength extracted from CCG peaks in V1 columns in mice[47] that reveal much strong increase of long-distance correlations between layer 2/3 and layer 5 during waking in comparison to sleep states. In general, not only brain state can modulate the connection strength, but most importantly, as shown in **Video 3** and **Fig.7A**, the connection strength between all the layers is strongly temporally modulated during the stimulus presentation. Therefore, our results demonstrate that tracking dynamic connectivity patterns in local cortical networks can be invaluable in assessing circuit-level dynamic network organization.

Dynamic connectivity along the hierarchy axis of all visual cortices

Similarly, cellular-level dynamic interactions at the cortex-wide level for all 6 cortical areas learned from all 26 sessions are shown in **Video 4**. Still frames from this Video for the same characteristic times are shown in **Fig.7B**. Inter-areal long-range interactions across various visual cortices (off-diagonal terms in **Fig.7B**) exhibit complex temporal evolution with rich feedforward (along the anatomical hierarchical score difference[5]) and feedback interactions. Therefore, DyNetCP can uncover the dynamics of feedforward- and feedback-dominated epochs during sensory stimulation, as well as behavioral states (e.g., epochs in the VCN dataset when animals are running or sitting), however, as opposed to population decoding models[26–29], produce cellular-level cell-type specific connectivity patterns that are otherwise hidden from analysis.

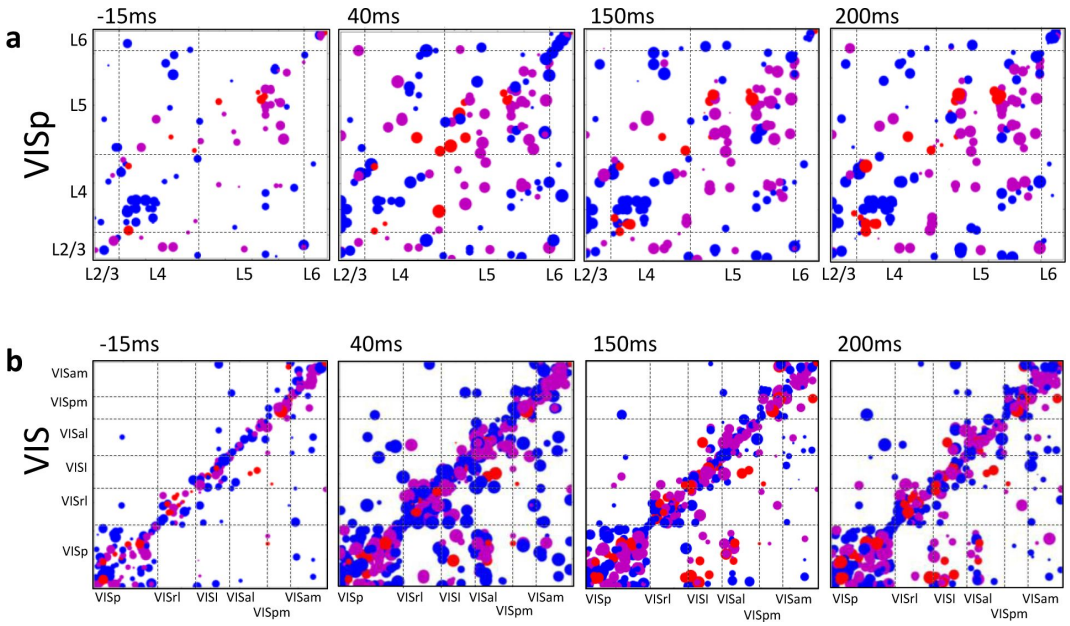

Figure 7.

Dynamic functional connectivity prediction along the hierarchy axis of visual cortices.

A $\mathbf{W_{off}}$ at different trial times (VISp area, n=26 animals). Units ordered by cortical depth and assigned to layers. The circles diameter is proportional to the dynamic offset. Red, blue, and magenta circles correspond to excitatory-excitatory, inhibitory-inhibitory, and mixed connections, respectively. **B)** $\mathbf{W_{off}}$ matrices for all visual areas (n=26 animals) ordered by their hierarchical

Discussion

DyNetCP can reveal cellular-level dynamic interactions within local circuits, within a single brain area, as well as across global hierarchically organized information pathways. Such detailed information, although present in the original datasets, is otherwise hidden from usual analysis that typically relies on time-averaged spike rate coding or population-averaged coding.

Biological interpretation of the extracted dynamic weights can follow the terminology of the short-term plasticity between synaptically connected neurons[25,33–37] or spike transmission strength[30–32,47]. Alternatively, temporal changes in connection weights can be interpreted in terms of dynamically reconfigurable functional interactions of cortical networks[8–11,13,46] through which the information is flowing. We could also not exclude interpretation that combines both ideas. In any event our goal here is to extract these signals for a pair (**video1**, **Fig.4**), a cortical local circuit (**Video 2**, **Fig.5**), and for the whole visual cortical network (**Videos 3**, **4** and **Fig.7**). We envision that the next step here, falling beyond the scope of the current paper, would be to correlate the time dependence of the extracted dynamic weights with the stimulus presentation and the dynamics of the behavioral parameters during the decision-making process to infer where and how the information is flowing in the timescale of a decision making.

It is instructional to assess whether the temporal cellular-level interactions uncovered by DyNetCP are bringing new latent dimensions to the analysis of neural code. Dimensionality reduction methods[18,43,48] are often used to estimate the number of independent dimensions of the code that can better explain the variability of spike trains. When principal component (PC) dimensionality reduction[29] is applied to the dynamic weights $\mathbf{W_{dyn}}$ of all valid pairs (i.e., passed through all 3 thresholds) in a single animal (65 units, 105 pairs, session 831882777), up to 33 components are required to account for 95% of the variance (**Fig.8A**, black). In contrast, only 5 PC are sufficient to explain 95% variance of spike rates for the same units (**Fig.8A**, red). If all clean units in all visual cortices are taken (264 VIS units) the dimensionality increases, but only slightly to 8 PC (**Fig.8A**, blue). The normalized intrinsic dimensionality (NID) estimated as a number of major PC components divided by the number of units is between 0.03 and 0.08 for spike rates exhibiting striking simplicity consistent with an often observed trend[49]. However, in contrast, the NID for dynamic weights is as large as 0.5 showing dramatic increase of dimensionality.

This result holds for each of the 26 sessions with the NID in the spiking rate space for valid pairs (**Fig.8B**, green, mean:0.20±0.018 SEM) and for all VIS units (**Fig.8B**, violet, mean:0.08±0.01 SEM). In contrast, much larger NID is observed in the space of dynamic weights (**Fig.8B**, orange, mean:0.55±0.02 SEM) indicating that the dimensionality of a dynamic network manifold is becoming comparable to the number of recorded units. Hence the observed complexity stems from a relatively small subpopulation (valid units in pairs mean: 42.7±3.3 SEM) comprising just 20% of the total (all clean VIS units mean: 194.9±11.9 SEM) and at relatively short time scales below 30ms when it survives temporal Gaussian kernel smoothing (inset in **Fig.8A**). DyNetCP, therefore, reveals the dynamically reconfigurable functional architecture of cortical networks that is otherwise hidden from analysis.

In summary, DyNetCP provides a fully reproducible and generalizable processing framework that allows investigators to explore often overlooked dimensions of the neural code that are potentially rich for novel biological insights. We believe that our approach can help to provide a conceptual link between brain-wide network dynamics studied with neuroimaging methods and modern electrophysiology approaches resolving such dynamics at a cellular level.

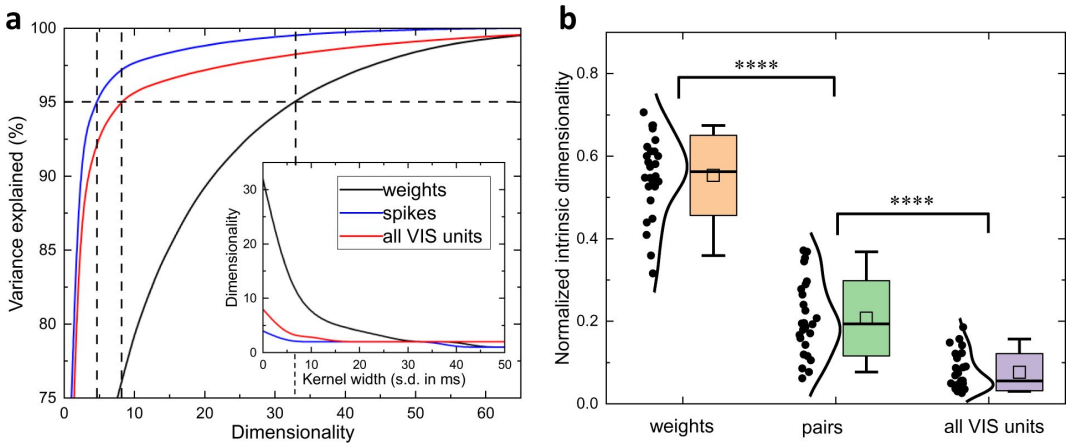

Figure 8.

Intrinsic dimensionality of dynamic connectivity is large

A) Intrinsic dimensionality of neural activity manifold (session 831882777, no temporal smoothing) using spiking data for all VIS cortical units (red), units in selected pairs (blue), and for the same unit pairs using dynamic weights (black). **Inset**: Intrinsic dimensionality as a function of temporal gaussian kernel width. B**)** Intrinsic dimensionality (n=26 animals) in spike rate space normalized by the number of all VIS units (violet) and units in selected pairs (green). Intrinsic dimensionality in a weight space for units in selected pairs (orange). Box: SD, whiskers: 5%-95% range, box: mean, horizontal line: median, distribution: kernel Scott, **** is p-value<0.0001.

Methods

1. Model implementation and training

Computational resources

The DyNetCP model can be trained in a single step to produce both static and dynamic weight matrices simultaneously. Alternatively, static, and dynamic training can be done sequentially to minimize the computational resources and to enable intermediate checking of the model parameters with respect to descriptive statistical results. In this case, prior to implementing the dynamic part of DyNetCP, the pairs are classified as putative connections based on a statistical analysis (see below) of the static weights, and the dynamic component is trained only on these pairs.

Computation time and memory consumption can also be optimized by the choice of the bin size d at the cost of temporal precision of the weight prediction. To better identify putative connections and to ease comparison with descriptive CCG models, we use a bin size of 1ms for training of static weights. For training the dynamic part, we use spiking data binned at a 5ms resolution. Evaluation of statistical significance of the model predictions (see below) indicates that a 5ms bin size strikes a good balance between computational efficiency, temporal resolution, and data sparsity.

All models are trained using the ADAM optimizer[50], a batch size of 16, and a learning rate of 0.0001 for 2000 epochs, where the learning rate is reduced by a factor of 10 after 1000 epochs. For each dataset, we set aside some of the data for validation. We use the validation data for early stopping: after every epoch of training, we compute the loss on the validation data, and terminate training early if the validation loss has not improved for a specific number of epochs (100 when training the static portion and 50 when training the dynamic portion). Note, to properly assess generalization, all plots in this work show DyNetCP static and dynamic weights outputs from the validation data.

When training the static part of the model on the synthetic HH dataset[25], we use $\lambda = 1$. For training the static part on the VCN dataset[15] we use $\lambda = 100$, which we found to lead to a lower residual when comparing to CCG values. For training the dynamic weights for all models we use $\lambda = 10$.

Averaging Dynamic Weights

To extract a strong signal from the DyNetCP dynamic weights, we need to aggregate information over experimental trials. However, we do not want to simply average the weights over trials, as all weights which are not paired with an incoming spike (i.e., all weights $w^{d}_{j\to i}$ such that $x_j^{t-d} = 0$) do not contribute to the spike rate prediction and therefore are not constrained to capture the spiking correlations. As a result, when computing trial-aggregated DyNetCP weights, we average over weights that are time-aligned with spike times of corresponding unit (**Fig.9A**) as follows:

$$\tilde{w}^{d,t}_{j\to i} = \frac{1}{\sum_{m=1}^{M}\mathbf{1}[X(m,j,t)=1]}\sum_{m=1}^{M}\mathbf{1}[X(m,j,t)=1]w^{d,t}_{j\to i} \qquad \text{Eq.9}$$

Additionally, to compensate for the sparsity of spiking, we average these aggregated dynamic weights over the 10 most recent bins (**Fig.9B**).

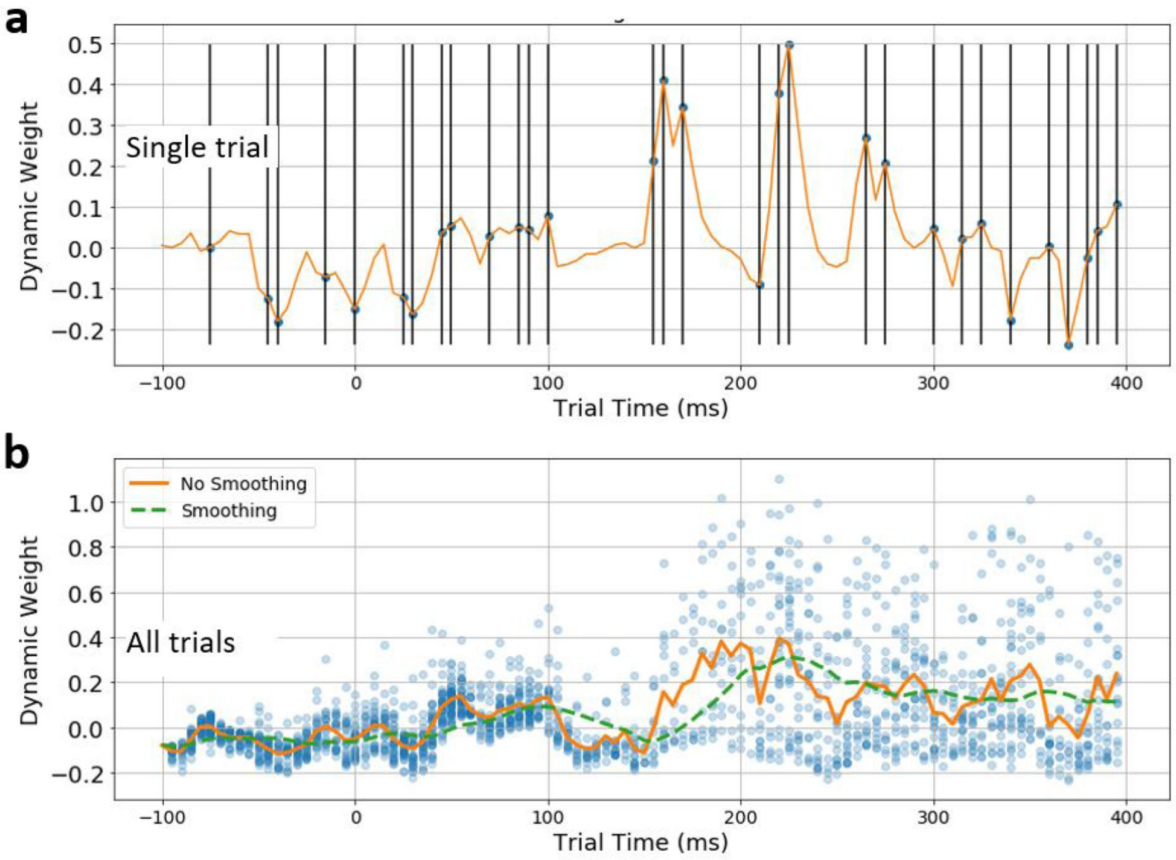

Fig. 9.

Selection of dynamic weight values and weights averaging

A) Selection of weights which contribute to averaging. Single trial spiking times for a given unit (black bars). Inferred dynamic weight values (orange curve) are selected at times when associated unit spikes (black dots), as the remaining weights do not contribute to the predicted spiking probability and therefore are not supervised to represent a meaningful value. **B) Averaging of weights**. Each blue point corresponds to a dynamic weight from a single trial. The orange curve represents a trial-average of every weight time-aligned with spikes. Green curve represents the Gaussian smoothing with a kernel including the 10 most recent bins.

Jitter correction

Jittering method [15,30,41–43] is often used in analysis of pairwise spiking correlations to minimize the influence of a potential stimulus-locked joint variation in population spiking that often occurs due to common input from many shared presynaptic neurons. To lessen the impact of such false positive (FP) connections in DyNetCP results and to ease the comparison with classical jitter-corrected CCG, we train a second static model on a jitter-corrected version of the data generated using a pattern jitter algorithm[41] with a jitter window of 25ms. When the dataset is trial-aligned (e.g. VCN dataset), we use the correction procedure[41] which determines the probability of a spike being present in each bin for all possible random shuffles of spikes among trials. For data which is not trial-aligned (e.g. synthetic dataset of HH neurons[25]), we randomly permute the spike times within the interval [−5ms, +5ms] before every weight update. New spike resampling is performed during every epoch of training. To assess putative connectivity, the jitter-corrected static weights $w'_{j\to i}$ produced by a jitter-corrected model are subtracted from the weights $w_{j\to i}$ trained on the original data to obtain $w^*_{j\to i} = w_{j\to i} - w'_{j\to i}$ and $w^*_{i\to j} = w_{i\to j} - w'_{i\to j}$.

2. Datasets

Synthetic network of HH neurons

We use a synthetic dataset consisting of Hodgkin-Huxley (HH) 800 excitatory and 200 inhibitory neurons with known ground truth (GT) synaptic connections[25]. The excitatory neurons influence 12.5% and the inhibitory neurons influence 25% of other neurons. We use the first 4320s of the 5400s-long data for training and the remaining 1080s for validation. Since DyNetCP requires training with trial-aligned data, we split each of these datasets into 1s "trials" consisting of 1 bins each. For training and evaluation we use spikes from the same subset of 20 excitatory neurons as was used for GLMCC validation[25] (**Fig.2.C,D,E**).

Synthetic dataset with FP connections

Synchronous spiking at short time lags does not necessarily indicate a direct connection but can also be induced by a shared common input (**Fig.10A**) or an indirect serial chain connection (**Fig.10B**) among others. While it is notoriously difficult to distinguish these confounding correlations using descriptive statistical models[24], the DyNetCP being a probabilistic model might lessen their impact by abstracting out such co-variates that do not contribute significantly to a prediction. To test the ability of DyNetCP to identify such confounds, we generate a synthetic dataset with known GT static and dynamic connectivity. The dataset consists of 100 excitatory neurons with their spikes generated by independent sampling from a Bernoulli distribution with spike rate between 0.002 and 0.01 per bin. The GT connection is active when spikes in neuron n_1 at time t are followed by spikes in neuron n_2 at a time $t + d$ with a probability of 0.6. Randomly generated 1 "triplets" emulating common input and serial chain connections are added to the pool. he "triplets" are active either during the first and last 1 5 bin period or only during the middle 5 bin period. DyNetCP trained on this dataset (400 train and 200 validation trials, each 500 bins long) enables comparison of static and dynamic weights (**Fig.10**) that indicate that when the GT connection is present the $\mathbf{W_{dyn}}$ tends to be larger than $\mathbf{W_{st}}$, which enables classification of connections as TP and FP for both common input (**Fig.10A**) and serial chain (**Fig.10B**) connections for this synthetic dataset.

Experimental dataset recorded in visual cortex

To demonstrate DyNetCP performance with in-vivo high-density electrophysiological recordings, we used the publicly available Allen Brain Observatory-Visual Coding Neuropixels (VCN) database[15] that contains spiking activity collected across 99,180 units from 6 different visual cortical areas in 58 awake mice viewing diverse visual stimuli. We use a "functional connectivity"

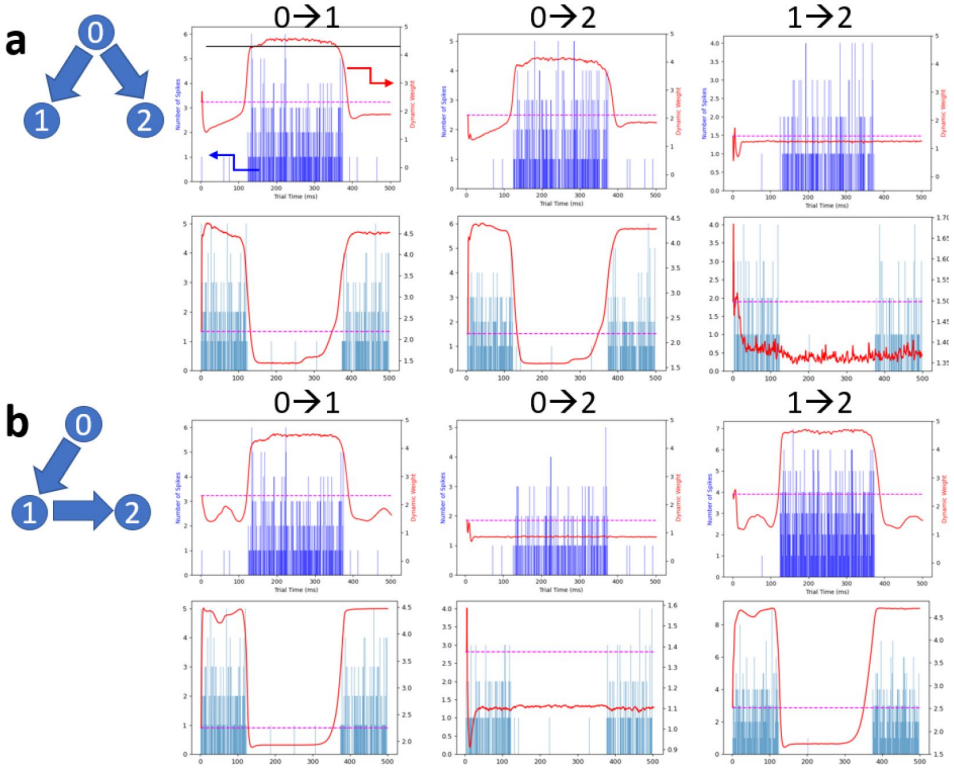

Fig. 10.

Performance of the model on synthetic dataset with FP connections

A) Identification of FP connections for a "common input" triplet. **Inset:** schematics of a triplet with common input from the unit 0 to both units 1 and 2. **Top row:** connection is active during the first and last 125 bin period of the trial. **Bottom row:** Connection is active only during the middle 375 bin period. Blue bars (left y-axis) represent a histogram of joint spiking probability (JPSTH anti-diagonal). Red curves correspond to inferred dynamic weights (right y-axis), while dotted magenta line represents static weight value. Comparison of dynamic and static weights might help to distinguish TP connections 0→1 and 0→2 from an artifactual FP connection 1→2. **B) Identification of FP connections for a "serial input" triplet**. **Inset:** schematics of a triplet with serial input from the unit 0 to 1 followed by 1 to 2. **Top row:** connection is active during the first and last 125 bin period of the trial. **Bottom row:** Blue bars (left y-axis) represent a histogram of joint spiking probability (JPSTH anti-diagonal). Red curves correspond to inferred dynamic weights (right y-axis), while dotted magenta line represents static weight value. Comparison of dynamic and static weights may help to distinguish TP connections 0→1 and 1→2 from an artifactual FP connection 0→2.

subset of these recordings corresponding to the “drifting grating 5 repeats” setting recorded for animals (26 sessions in **Table 1**). Full-field drifting grating stimuli was passively viewed by a head-fixed animal freely running on a treadmill[15]. Stimuli consists of 2s presentation of drifting diffraction grating (temporal frequency 2 cycles/s, spatial frequency = 0.04 cycles per degree) that is interleaved with a 1s grey period (top left inset in **Fig.1A**). Presentation of gratings were repeated 75 times per orientation (0, 45, 90, and 135 degrees) and per contrast (0.8 and 0.4). To maximize the number of spikes available for training we use all angles and all contrast trials.

We split the 600 total experimental trials for each session into 480 training and 120 validation trials by selecting 60 training trials from each configuration of contrast or grating angle and 15 for validation. To further investigate the influence of brain state on connectivity dynamics we identify in each session trials with the average running speed above 5cm/s that are mar ed as “running”. he rest of the trials are mar ed as “not running”. When trained and validated, the model results can then be analyzed and compared for “running” vs “non-running” conditions separately.

Models used

GLMCC model

Python code for GLMCC method is taken from the author’s version[51]. For these experiments, we use the synthetic dataset of interconnected HH neurons[25]. We focus specifically on recovering ground-truth (*GT*) excitatory connections. To facilitate a comparison with GLMCC model[25], we here choose thresholds α_w, α_s, and α_p to maximize the Matthews Correlation Coefficient (MCC, Eq.9). MCC optimization balances between maximizing the number of *TP* pairs recovered while minimizing the number of *FP* pairs which are predicted.

Since a predicted connection is counted as a *TP* only once (i.e., $i \rightarrow j$ and $j \rightarrow i$ do not count as two negatives if i is not connected to j) and the number of *GT* connections decreases when α_p increases, the MCC exhibits an increase beyond α_p=100. A more detailed analysis of TP and FP rates as a function of pair spike threshold is presented in **Fig.2 - figure supplement 1**.

Though GLMCC performs well in recovering static network structure, we emphasize that GLMCC is not compatible with modeling network dynamics and thus cannot be integrated into DyNetCP. Specifically, our goal is to model the correlations of spiking of a network of neurons and track the changes of these correlations across time. GLMCC learns correlations as a function of the time lag relative to the spiking time of a reference neuron. It is hence unable to link correlations to specific moments in a trial time. Therefore, it cannot represent the dynamics of correlations, preventing its use in analysis of network activity relative to subject behavior.

Conditional Joint Peristimulus Time Histogram (cJPSTH)

The Joint Peristimulus Time Histogram (JPSTH) is a classical tool[39] used to analyze the joint correlations of spiking behavior between two neurons and their variation across time. For a proper comparison with conditional DyNetCP results, we use a conditional joint peristimulus time histogram (cJPSTH), where we divide the columns of the JPSTH by the PSTH of neuron i (**Fig.4B,C**). Due to the sparsity of spiking in the data we use, it is beneficial to average the entries of the cJPSTH over short windows in time to more clearly extract the dynamics of the correlations between neurons. Specifically, we replace each entry (a, b) in the cJPSTH by the average of the T most recent bins having the same delay $a - b$, that is,

$$cJPSTH_{Avg}(a,b) = \frac{1}{T}\sum_{i=0}^{T-1} cJPSTH(a-i, b-i) \qquad \text{Eq.10}$$

For most of the comparisons we use T=10 bins. Note that for most cJPSTH plots (e.g., **Fig.4E**), to directly compare to DyNetCP plots (e.g., **Fig.4D**), we only show data representing the "upper diagonal" of the full plot which represents data where neuron i spikes at the same time or before neuron j spikes. Specific implementation and comparisons of both models can be found in the accompanying Jupyter Notebook.

Dimensionality reduction

Dimensionality reduction[18,43,48] is based on calculating principal components (PC) on the dataset and estimating the data variance that can be explained by a minimal number of PC. The dimensionality reduction code following a standard PCA reduction method[48] is rewritten in Python and is used for analysis in **Fig. 8A,B**.

4. Statistical analysis of filtering and classification of units and pairs

The total number of units (raw units) recorded from visual cortices in 26 sessions of the VCN dataset[15] is 18168. Units and pairs are filtered and classified by the following procedure.

Unit quality metrics

First, we apply standard unit quality metrics[15] including amplitude cutoff < 0.1; violations of inter-spike interval (ISI) < 0.1; presence ratio > 0.95; isolation distance > 30; and signal to noise ratio (snr) > 1. This results in 5067 units (clean units).

Static weight peak threshold

Second, short-latency peaks within the first 10ms in the $w^*_{j\to i}$ and $w^*_{i\to j}$ of static weights are examined (example analysis for session 771160300 is shown **Fig.2A,B**). Following the accepted approach[15,19,21,25,30] a putative connection is considered statistically significant when the magnitude of the peak exceeds a certain peak weight threshold α_w measured in units of standard deviations (SD) of the noise in the flanks, calculated within [51ms, 100ms] from both directions $w^*_{i\to j}$ and $w^*_{i\to j}$. When pairs are filtered with increasing peak weight threshold α_w (**Fig.11A**), the number of corresponding valid units is fast decreasing (black curve). For all 26 sessions 5067 clean units participate in formation of 5203 pairs with noticeable weight peaks. Filtering them using α_w=7SD results in 1680 pairs corresponding to 1102 units. Close examination of these pairs (example analysis for session 771160300 is shown in **Fig.11A**) reveals that units not only form pairs (violet curve), but also form triplets (green), quintuplets (blue), and even participate in connections above 10-tuples (red). High radix hubs of this type are most likely FP artefacts imposed by sparse spiking (see below) and need to be filtered out. Indeed, electrophysiology spiking datasets are typically very sparse, with many interesting units often generating spikes at rates below 1Hz. Increasing the threshold α_w does help to filter out high radix connections, but still even for α_w as large as 8 there is a substantial number of units participating in connections larger than 3.

Unit spike rate

Therefore, as a third filtering step, we apply a unit spike rate threshold α_s to limit the minimal spike rate to 1Hz.

Pair spike rate threshold

It has been argued[25] that, to reliably infer that a connection is present (i.e. to disprove the null hypothesis that a connection is absent), each binned time interval in the CCG histogram d should contain a sufficiently large number of spikes from both participating units. This implies that the

spike rate of each neuron in a pair λ_i and λ_j should exceed the threshold α_s, and the joint number of spikes in each time bin should exceed the pair spike threshold, defined as

$$\alpha_p = \lambda_i \lambda_j TMd. \quad \text{Eq.11}$$

The confidence interval for a null hypothesis that two spike trains are independent stationary Poisson processes[25] is then defined as

$$J_{\mp} = \sqrt{\alpha_p}. \quad \text{Eq.12}$$

To disprove the null hypothesis and infer that a connection is statistically significant, α_p should exceed[25] 10. To train the dynamic DyNetCP we use recordings binned at d of 5ms repeated over M of 480 randomized trials and the dynamic weights are influenced by T=10 most recent bins (**Fig.9B**). This corresponds to the TMd product of 24 that implies the minimum joint pair spike rate $\lambda_i\lambda_j$ of 0.41s^{-2}. This threshold, however, might be insufficient for inference of the dynamic weight since only spikes within a short trial time interval are being used for learning. Indeed, analysis of an example pair (**Fig.12A**) that passed the α_w=7SD threshold and has $\lambda_i\lambda_j$ = 0.73s^{-2}, reveals that it exhibits on average just 2 spikes per trial or a total of 272 spikes for all 480 trials in a 500ms trial time window of interest. Corresponding jitter-corrected static weight matrix (**Fig.12A**, left) and cJPSTH (**Fig.12A**, bottom right) are very sparsely populated. The dynamic weight matrix (right top), although it is reproducing this sparseness, is not statistically convincing. Moreover, such pairs contribute significantly to high radix tuples.

By increasing the $\lambda_i\lambda_j$ pair spike rate threshold, the number of high radix tuples is decreasing (example analysis for session 771160300 is shown in **Fig.11B**), however the α_p threshold alone is not sufficient to eliminate them. Hence, for a given pair to be classified as a putative connection, the classification procedure requires the use of all three thresholds: α_w, α_s, and α_p (see Jupyter Notebook for specific implementation).

Choice of thresholds

When all three thresholds α_s, α_w and α_p are applied simultaneously (**Fig.11C**) the number of valid units is decreasing rapidly with the increase of α_w to 7SD and $\lambda_i\lambda_j$ beyond 10 with slower decrease at higher thresholds. Examination of an example pair with joint pair spiking rate $\lambda_i\lambda_j$ of 50 s^{-2} (**Fig.12B**) indicates that while the static weight matrix shows a prominent (α_w >7SD) small latency peak, the cJPSTH is still populated relatively sparsely and the dynamic weight matrix resembles it much less (r_p=0.27). In contrast, for an example pair with joint pair spiking rate $\lambda_i\lambda_j$ of 130 s^{-2} (**Fig.12C**) the resemblance between cJPSTH and the dynamic weight matrix is striking (r_p=0.82, P_p<0.001).

For a fixed α_s of 1Hz and α_w of 7SD the distribution of all valid pairs with respect to their joint spike rates (**Fig.13A**) shows a maximum around $\lambda_i\lambda_j$=200 s^{-2} with a long tail to higher rates. To be conservative, for all the analysis of the inferred connectivity patterns in this work, we used $\lambda_i\lambda_j$ of 200 s^{-2} (α_p=4800, red arrow in **Fig.13A**).

Application of all 3 filters to all 26 sessions produces 808 units forming 1020 pairs (**Table 1**) with distribution of inferred static and dynamic weights shown in **Fig.13B**.

Units' classification

Once all pairs are filtered, the directionality is assigned to each putative connection, either $j \rightarrow i$ or $i \rightarrow j$, that is identified by the functional delay of the static weight peak binned at 1ms. Cortical depth perpendicular to cortical surface is calculated from unit coordinates in ccfv3 format (Allen Mouse Brain Common Coordinate Framework [52]). Layer assignment is performed following method[15] using units coordinates in the ccfv3 framewor and the annotation matri with

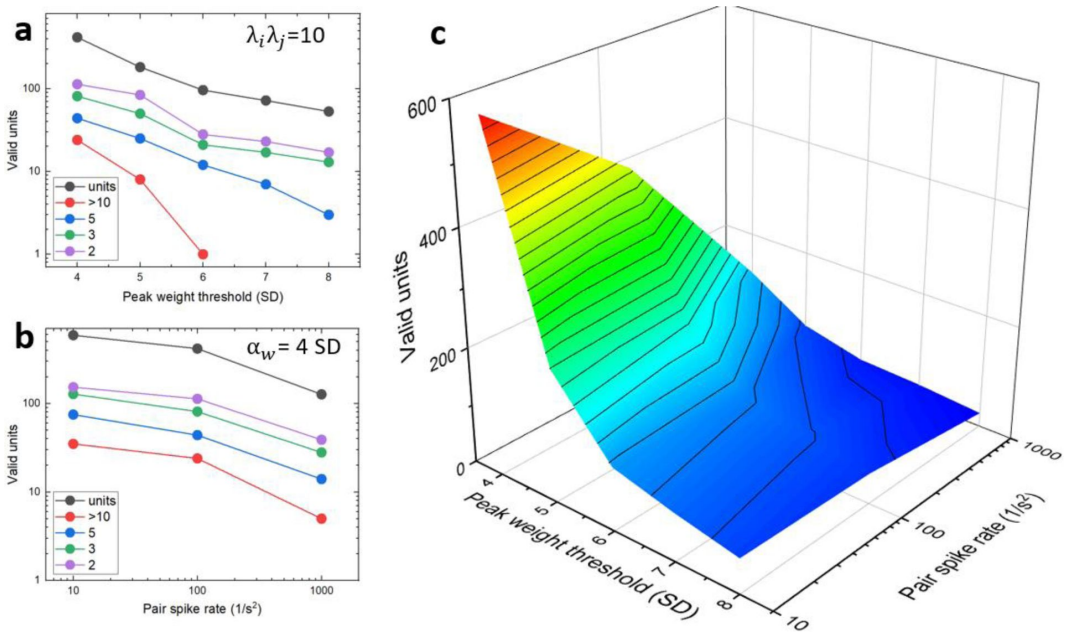

Fig. 11.

Thresholds for units and pairs filtering

A) Number of valid units (session #771160300) that form pairs with distinct static peak (black curve) for different peak weight thresholds. Violet, green, blue, and red curves correspond to units that participate in formation of pairs, triplets, quintuplets, and connections above 10-tuples, correspondingly. **B)** Number of valid units that form pairs with static peak above 4SD (black curve) for different pair spike rate. Violet, green, blue, and red curves correspond to units that participate in formation of pairs, triplets, quintuplets, and connections above 10-tuples, correspondingly. **C)** 3D plot of a number of valid units that form pairs for different peak thresholds and pair spike rates.

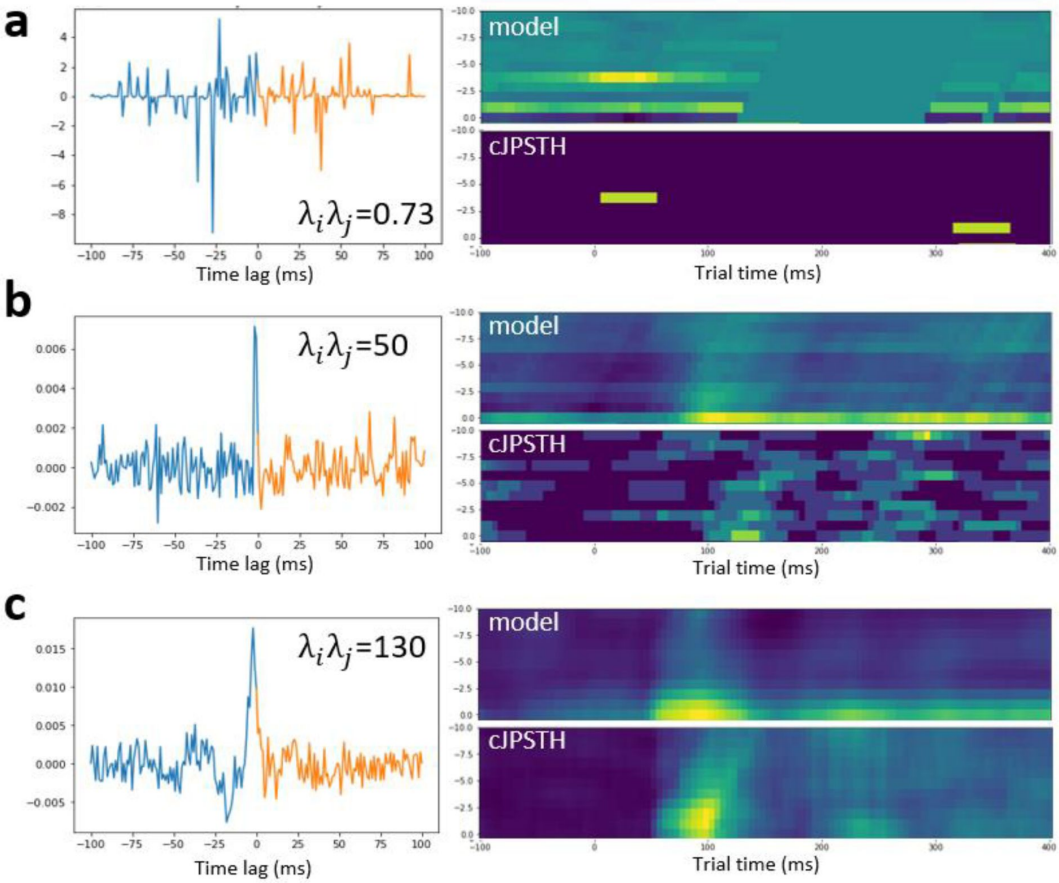

Fig. 12.

Example of pairs and dynamic model performance

A) Example of a pair of units (session #771160300, excitatory units from VISam and VISpm areas with spike rates 1.92Hz and 0.35Hz) that pass a peak weight threshold of 7SD (left static weight matrix plot), however, has pair spike rate as small as 0.73 s^{-2}. Corresponding cJPSTH (bottom right) and dynamic weight plots (top right) are sparse. **B)** Example of a pair of units (session #771160300, excitatory VISp unit with 7.2Hz spike rate and inhibitory VISp unit with 6.8Hz rate) that pass a peak weight threshold of 7SD (left static weight plot), however, has moderate pair spike rate of 50 s^{-2}. Corresponding cJPSTH and dynamic weight plots are shown on the right. **C)** Example of a pair of units that pass peak weight threshold of 7SD (left static weight plot), that has a relatively high pair spike rate of 130 s^{-2}. Corresponding cJPSTH and dynamic weight plots are shown on the right.

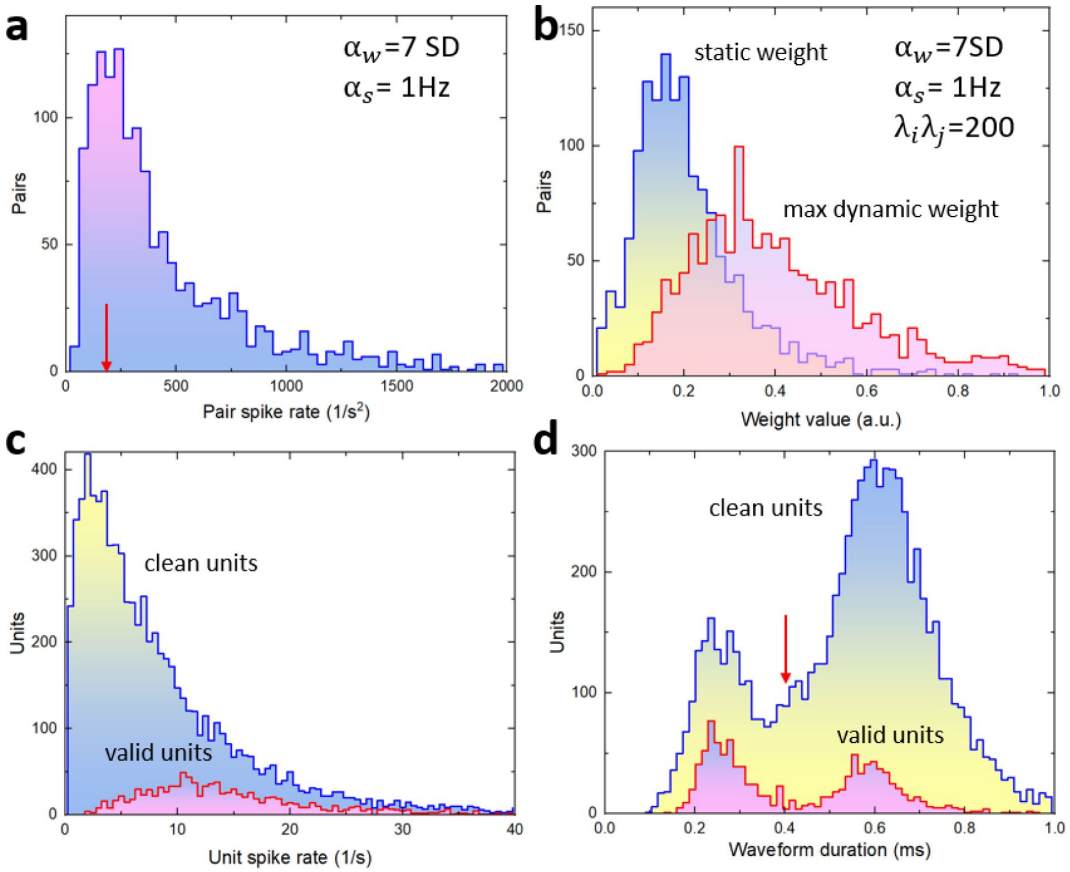

Fig. 13.

Filtered pairs and potential biases.

A) Histogram of pairs recorded in all VIS cortices for all 26 animals that pass 7SD peak weight threshold and are formed from units with spike rate exceeding 1Hz. Red arrow shows the pair spike threshold of 200 s^{-2}. **B)** Histograms of inferred static and maximum dynamic weights for filtered pairs. **C)** Histograms of unit spike rates for clean units and for valid units belonging to filtered pairs. **D)** Histograms of waveform duration for clean units and valid units. Red arrow indicates a threshold to classify units as inhibitory or excitatory.

reference space ey 'annotation/ccf_ 1'. All units are classified as excitatory if their waveform duration is longer than 0.4ms and the rest as inhibitory (**Fig.13D**). Since transgenic mice were used for some of the sessions in the VCN dataset, optical activation of light-gated ion channel (in this case, ChR2) in Cre+ neurons with light pulses delivered to the cortical surface generate precisely time-aligned spikes that enable to link spike trains to genetically defined cell classes. Optical tagging was used to further classify inhibitory units[45] as Parvalbumin-positive neurons (Pvalb), Somatostatin-positive neurons (Sst), and Vasoactive Intestinal Polypeptide neurons (Vip).

Potential biases

The statistical analysis and filtering procedure described above is biased towards strongly spiking units (**Fig.13C**) and as such can generate certain biases in connectivity patterns. For example, inhibitory units constitute about 18% of all 5067 clean units that pass unit quality metrics (**Fig.13D**). However, after filtering down to 808 valid units, they constitute over 50% of the population (**Fig.13D**). In general, inhibitory units have a higher spiking rate (for all clean units mean: 15.4Hz±0.29 SEM) than excitatory (mean: 6.3Hz±0.08 SEM). This might explain, at least partially, the over-representation of connections involving inhibitory units in the dynamic connectivity plots.

Data Availability

All of the datasets used in this article are publicly available online under the Creative Commons Attribution 4.0 International license. Synthetic data of interconnected HH neurons[25] is available at figshare[53] (*https://doi.org/10.6084/m9.figshare.9637904*). The Allen Brain Observatory-Visual Coding Neuropixels (VCN) database[15] is available for download in Neurodata Without Borders (NWB) format via the AllenSDK. The NWB files are available as an AWS public dataset (*https://registry.opendata.aws/allen-brain-observatory/*). Synthetic dataset with artifactual FP connections as well as trained static and dynamic weights for all 26 sessions of VCN database are availabel at Figshare *https://doi.org/10.6084/m9.figshare.24879036*

Code Availability

DyNetCP introduced and used in this article is open-source software (GNU General Public License v3.0). The source code is available in a GitHub repository (*https://github.com/NeuroTechnologies/DyNetCP*) that contains codes for model training as well as a Jupyter notebook for generating the results used in the paper and in the SM.

References

1 Hubel D. H., Wiesel T. N. (1962) **Receptive fields, binocular interaction and functional architecture in the cat's visual cortex** *J Physiol* **160**:106–154 https://doi.org/10.1113/jphysiol.1962.sp006837

2 Mahalingam G., et al. (2022) **A scalable and modular automated pipeline for stitching of large electron microscopy datasets** *eLife* **11** https://doi.org/10.7554/eLife.76534

3 Hawrylycz M. J., et al. (2012) **An anatomically comprehensive atlas of the adult human brain transcriptome** *Nature* **489**:391–399 https://doi.org/10.1038/nature11405

4 Oh S. W., et al. (2014) **A mesoscale connectome of the mouse brain** *Nature* **508**:207–214 https://doi.org/10.1038/nature13186

5 Harris J. A., et al. (2019) **Hierarchical organization of cortical and thalamic connectivity** *Nature* **575**:195–202 https://doi.org/10.1038/s41586-019-1716-z

6 Sporns O., Tononi G., Kötter R. (2005) **The Human Connectome: A Structural Description of the Human Brain** *PLOS Computational Biology* **1** https://doi.org/10.1371/journal.pcbi.0010042

7 Calhoun Vince D., Miller R., Pearlson G., Adalı T. (2014) **The Chronnectome: Time-Varying Connectivity Networks as the Next Frontier in fMRI Data Discovery** *Neuron* **84**:262–274 https://doi.org/10.1016/j.neuron.2014.10.015

8 Bassett D. S., Yang M., Wymbs N. F., Grafton S. T. (2015) **Learning-induced autonomy of sensorimotor systems** *Nature Neuroscience* **18**:744–751 https://doi.org/10.1038/nn.3993

9 Cole Michael W., Bassett Danielle S., Power Jonathan D., Braver Todd S., Petersen Steven E. (2014) **Intrinsic and Task-Evoked Network Architectures of the Human Brain** *Neuron* **83**:238–251 https://doi.org/10.1016/j.neuron.2014.05.014

10 Shine James M., et al. (2016) **The Dynamics of Functional Brain Networks: Integrated Network States during Cognitive Task Performance** *Neuron* **92**:544–554 https://doi.org/10.1016/j.neuron.2016.09.018

11 Shine J. M., et al. (2019) **Human cognition involves the dynamic integration of neural activity and neuromodulatory systems** *Nature Neuroscience* **22**:289–296 https://doi.org/10.1038/s41593-018-0312-0

12 Shen K., Hutchison R. M., Bezgin G., Everling S., McIntosh A. R. (2015) **Network Structure Shapes Spontaneous Functional Connectivity Dynamics** *The Journal of Neuroscience* **35** https://doi.org/10.1523/JNEUROSCI.4903-14.2015

13 Nozari E., et al. (2024) **Macroscopic resting-state brain dynamics are best described by linear models** *Nature Biomedical Engineering* **8**:68–84 https://doi.org/10.1038/s41551-023-01117-y

14 Jun J. J., et al. (2017) **Fully integrated silicon probes for high-density recording of neural activity** *Nature* **551**:232–236 https://doi.org/10.1038/nature24636

15 Siegle J. H., et al. (2021) **Survey of spiking in the mouse visual system reveals functional hierarchy** *Nature* https://doi.org/10.1038/s41586-020-03171-x

16 Sofroniew N. J., Flickinger D., King J., Svoboda K. (2016) **A large field of view two-photon mesoscope with subcellular resolution for in vivo imaging** *eLife* **5** https://doi.org/10.7554/eLife.14472

17 Engel T. A., Schölvinck M. L., Lewis C. M. (2021) **The diversity and specificity of functional connectivity across spatial and temporal scales** *NeuroImage* **245** https://doi.org/10.1016/j.neuroimage.2021.118692

18 Engel T. A., Steinmetz N. A. (2019) **New perspectives on dimensionality and variability from large-scale cortical dynamics** *Current Opinion in Neurobiology* **58**:181–190 https://doi.org/10.1016/j.conb.2019.09.003

19 Jia X., et al. (2022) **Multi-regional module-based signal transmission in mouse visual cortex** *Neuron* **110**:1585–1598 https://doi.org/10.1016/j.neuron.2022.01.027

20 Semedo J. D., et al. (2022) **Feedforward and feedback interactions between visual cortical areas use different population activity patterns** *Nature Communications* **13** https://doi.org/10.1038/s41467-022-28552-w

21 Gokcen E., et al. (2022) **Disentangling the flow of signals between populations of neurons** *Nature Computational Science* **2**:512–525 https://doi.org/10.1038/s43588-022-00282-5

22 Okatan M., Wilson M. A., Brown E. N. (2005) **Analyzing Functional Connectivity Using a Network Likelihood Model of Ensemble Neural Spiking Activity** *Neural Computation* **17**:1927–1961 https://doi.org/10.1162/0899766054322973

23 Pillow J. W., et al. (2008) **Spatio-temporal correlations and visual signalling in a complete neuronal population** *Nature* **454**:995–999 https://doi.org/10.1038/nature07140

24 Stevenson I. H., Rebesco J. M., Miller L. E., Körding K. P. (2008) **Inferring functional connections between neurons** *Current Opinion in Neurobiology* **18**:582–588 https://doi.org/10.1016/j.conb.2008.11.005

25 Kobayashi R., et al. (2019) **Reconstructing neuronal circuitry from parallel spike trains** *Nature Communications* **10** https://doi.org/10.1038/s41467-019-12225-2

26 Pandarinath C., et al. (2018) **Inferring single-trial neural population dynamics using sequential auto-encoders** *Nature Methods* **15**:805–815 https://doi.org/10.1038/s41592-018-0109-9

27 Kaufman M. T., Churchland M. M., Ryu S. I., Shenoy K. V. (2014) **Cortical activity in the null space: permitting preparation without movement** *Nature Neuroscience* **17**:440–448 https://doi.org/10.1038/nn.3643

28 Keeley S. L., Zoltowski D. M., Aoi M. C., Pillow J. W. (2020) **Modeling statistical dependencies in multi-region spike train data** *Current Opinion in Neurobiology* **65**:194–202 https://doi.org/10.1016/j.conb.2020.11.005

29 Semedo J. D., Gokcen E., Machens C. K., Kohn A., Yu B. M. (2020) **Statistical methods for dissecting interactions between brain areas** *Current Opinion in Neurobiology* **65**:59–69 https://doi.org/10.1016/j.conb.2020.09.009

30 Fujisawa S., Amarasingham A., Harrison M. T., Buzsáki G. (2008) **Behavior-dependent short-term assembly dynamics in the medial prefrontal cortex** *Nature Neuroscience* **11**:823–833 https://doi.org/10.1038/nn.2134

31 English D. F., et al. (2017) **Pyramidal Cell-Interneuron Circuit Architecture and Dynamics in Hippocampal Networks** *Neuron* **96**:505–520 https://doi.org/10.1016/j.neuron.2017.09.033

32 McKenzie S., et al. (2021) **Preexisting hippocampal network dynamics constrain optogenetically induced place fields** *Neuron* **109**:1040–1054 https://doi.org/10.1016/j.neuron.2021.01.011

33 Ren N., Wei G., Ghanbari A., Stevenson I. H. (2022) **Predictable Fluctuations in Excitatory Synaptic Strength Due to Natural Variation in Presynaptic Firing Rate** *The Journal of Neuroscience* **42**:8608–8620 https://doi.org/10.1523/jneurosci.0808-22.2022

34 Stevenson I., Koerding K. (2011) **Inferring spike-timing-dependent plasticity from spike train data** *Advances in Neural Information Processing Systems* **24**

35 Linderman S., Stock C. H., Adams R. P. (2014) **A framework for studying synaptic plasticity with neural spike train data** *Advances in Neural Information Processing Systems* **27**

36 Robinson B. S., Berger T. W., Song D. (2016) **Identification of Stable Spike-Timing-Dependent Plasticity from Spiking Activity with Generalized Multilinear Modeling** *Neural Computation* **28**:2320–2351 https://doi.org/10.1162/NECO_a_00883

37 Wei G., Stevenson I. H. (2021) **Tracking Fast and Slow Changes in Synaptic Weights From Simultaneously Observed Pre- and Postsynaptic Spiking** *Neural Computation* **33**:2682–2709 https://doi.org/10.1162/neco_a_01426

38 Graber C., Loh R., Vlasov Y. A., Schwing A. (2019) **Proc. 33rd Annu. Conf. Neural Inf. Process. Syst**

39 Gerstein G. L. (2013) **Joint Peri Stimulus Time Histogram (JPSTH)** *Encyclopedia of Computational Neuroscience* :1–4 https://doi.org/10.1007/978-1-4614-7320-6_397-1

40 Tancik M., et al. (2020) **Fourier Features Let Networks Learn High Frequency Functions in Low Dimensional Domains** *arXiv e-prints* https://doi.org/10.48550/arXiv.2006.10739

41 Harrison M. T., Geman S. (2009) **A Rate and History-Preserving Resampling Algorithm for Neural Spike Trains** *Neural Computation* **21**:1244–1258 https://doi.org/10.1162/neco.2008.03-08-730

42 Amarasingham A., Harrison M. T., Hatsopoulos N. G., Geman S. (2012) **Conditional modeling and the jitter method of spike resampling** *J Neurophysiol* **107**:517–531 https://doi.org/10.1152/jn.00633.2011

43 Platkiewicz J., Saccomano Z., McKenzie S., English D., Amarasingham A. (2021) **Monosynaptic inference via finely-timed spikes** *J Comput Neurosci* **49**:131–157 https://doi.org/10.1007/s10827-020-00770-5

44 Brody C. D. (1999) **Correlations Without Synchrony** *Neural Computation* **11**:1537–1551 https://doi.org/10.1162/089976699300016133

45 Optotagging Analysis (2022) **Optotagging Analysis. Tutorial overview (https://allensdk.readthedocs.io/en/latest/_static/examples/nb/ecephys_optotagging.html, 2022).**

46 Trepka E. B., Zhu S., Xia R., Chen X., Moore T. (2022) **Functional interactions among neurons within single columns of macaque V1** *eLife* **11** https://doi.org/10.7554/eLife.79322

47 Senzai Y., Fernandez-Ruiz A., Buzsáki G. (2019) **Layer-Specific Physiological Features and Interlaminar Interactions in the Primary Visual Cortex of the Mouse** *Neuron* **101**:500–513 https://doi.org/10.1016/j.neuron.2018.12.009

48 Cowley B. R., et al. (2013) **DataHigh: graphical user interface for visualizing and interacting with high-dimensional neural activity** *Journal of Neural Engineering* **10** https://doi.org/10.1088/1741-2560/10/6/066012

49 Gao P., et al. (2017) **A theory of multineuronal dimensionality, dynamics and measurement** *bioRxiv* https://doi.org/10.1101/214262

50 Kingma D. P., Ba J. (2014) **Adam: A Method for Stochastic Optimization** *arXiv* https://doi.org/10.48550/arXiv.1412.6980

51 Kobayashi R., et al. (2019) **GLMCC: The generalized linear model for spike cross-correlation**

52 Wang Q., et al. (2020) **The Allen Mouse Brain Common Coordinate Framework: A 3D Reference Atlas** *Cell* **181**:936–953 https://doi.org/10.1016/j.cell.2020.04.007

53 Kobayashi R., et al. (2019) **Synthetic spike data generated by a network of 1000 hodgkin-huxley type neurons** *Figshare* https://doi.org/10.6084/m9.figshare.9637904

Editors

Reviewing Editor
Peter Latham
University College London, London, United Kingdom

Senior Editor
Timothy Behrens
University of Oxford, Oxford, United Kingdom

Reviewer #1 (Public review):

Summary:

This work proposes a new method, DyNetCP, for inferring dynamic functional connectivity between neurons from spike data. DyNetCP is based on a neural network model with a two-stage model architecture of static and dynamic functional connectivity.
This work evaluates the accuracy of the synaptic connectivity inference and shows that DyNetCP can infer the excitatory synaptic connectivity more accurately than a state-of-the-art model (GLMCC) by analyzing the simulated spike trains. Furthermore, it is shown that the inference results obtained by DyNetCP from large-scale in-vivo recordings are similar to the results obtained by the existing methods (jitter-corrected CCG and JPSTH). Finally, this work

investigates the dynamic connectivity in the primary visual area VISp and in the visual areas using DyNetCP.

Strengths:

The strength of the paper is that it proposes a method to extract the dynamics of functional connectivity from spike trains of multiple neurons. The method is potentially useful for analyzing parallel spike trains in general, as there are only a few methods (e.g. Aertsen et al., J. Neurophysiol., 1989, Shimazaki et al., PLoS Comput Biol 2012) that infer the dynamic connectivity from spikes. Furthermore, the approach of DyNetCP is different from the existing methods: while the proposed method is based on the neural network, the previous methods are based on either the descriptive statistics (JSPH) or the Ising model.

Weaknesses:

Although the paper proposes a new method, DyNetCP, for inferring the dynamic functional connectivity, its strengths are neither clear nor directly demonstrated in this paper. That is, insufficient analyses are performed to support the usefulness of DyNetCP.
First, this paper attempts to show the superiority of DyNetCP by comparing the performance of synaptic connectivity inference with GLMCC (Fig. 2). However, the improvement in the synaptic connectivity inference does not seem to be convincing. While this paper compares the performance of DyNetCP with a state-of-the-art method (GLMCC), there are several problems with the comparison. For example,

(1) It is unclear how accurately the proposed method can infer the dynamic connectivity.
(2) This paper does not compare with existing approach (e.g., classical JPSTH: Aertsen et al., J. Neurophysiol., 1989, and other methods : Stevenson and Koerding, NIPS, 2011; Linderman et al., NIPS, 2014; Song et al., J. Neurosci. Methods, 2015), and
(3) only a population of neurons generated from the Hodgkin-Huxley model was evaluated.

Thus, the results in this paper are not sufficient to conclude the superiority of DyNetCP in the estimation of synaptic connections. In addition, this paper compares the proposed method with the standard statistical methods Jitter-corrected CCG (Fig. 3) and JPSTH (Fig. 4). Unfortunately, these results do not show the superiority of the proposed method. It only shows that the results obtained by the proposed method are consistent with those obtained by the existing methods (CCG or JPSTH). This paper also compares the proposed method with the standard statistical methods, such as jitter-corrected CCG (Fig. 3) and JPSTH (Fig. 4). It only shows that the results obtained by the proposed method are consistent with those obtained by the existing methods (CCG or JPSTH), which does not show the superiority of the proposed method.

In summary, although DyNetCP has the potential to infer the dynamic (time-dependent) correlation more accurately than existing methods, the paper does not provide sufficient analysis to make this claim. It is also unclear whether the proposed method is superior to the existing methods for estimating functional connectivity, such as JPSTH and statistical approach (Stevenson and Koerding, NIPS, 2011; Linderman et al., NIPS, 2014). Thus, the strength of DyNetCP is unclear.

https://doi.org/10.7554/eLife.95449.2.sa2

Reviewer #2 (Public review):

Summary:

Here the authors describe a model for tracking time-varying coupling between neurons from multi-electrode spike recordings. Their approach extends a GLM with static coupling between

neurons to include dynamic weights, learned by a long-short-term-memory (LSTM) model. Each connection has a corresponding LSTM embedding and is read-out by a multi-layer perceptron to predict the time-varying weight.

Strengths:

This is an interesting approach to an open problem in neural data analysis. I think, in general, the method would be interesting to computational neuroscientists.

Weaknesses:

It is somewhat difficult to interpret what the model is doing. I think it would be worthwhile to add some additional results that make it more clear what types of patterns are being described and how.

Major Issues:

Simulation for dynamic connectivity. It certainly seems doable to simulate a recurrent spiking network whose weights change over time, and I think this would be a worthwhile validation for this DyNetCP model. In particular, I think it would be valuable to understand how much the model overfits, and how accurately it can track known changes in coupling strength. If the only goal is "smoothing" time-varying CCGs, there are much easier statistical methods to do this (c.f. McKenzie et al. Neuron, 2021. Ren, Wei, Ghanbari, Stevenson. J Neurosci, 2022), and simulations could be useful to illustrate what the model adds beyond smoothing.

Stimulus vs noise correlations. For studying correlations between neurons in sensory systems that are strongly driven by stimuli, it's common to use shuffling over trials to distinguish between stimulus correlations and "noise" correlations or putative synaptic connections. This would be a valuable comparison for Fig 5 to show if these are dynamic stimulus correlations or noise correlations. I would also suggest just plotting the CCGs calculated with a moving window to better illustrate how (and if) the dynamic weights differ from the data.

Minor Issues:

Introduction - it may be useful to mention that there have been some previous attempts to describe time-varying connectivity from spikes both with probabilistic models: Stevenson and Kording, Neurips (2011), Linderman, Stock, and Adams, Neurips (2014), Robinson, Berger, and Song, Neural Computation (2016), Wei and Stevenson, Neural Comp (2021) ... and with descriptive statistics: Fujisawa et al. Nat Neuroscience (2008), English et al. Neuron (2017), McKenzie et al. Neuron (2021).

In the sections "Static DyNetCP ...reproduce". It may be useful to have some additional context to interpret the CCG-DyNetCP correlations and CCG-GLMCC correlations (for simulation). If I understand right, these are on training data (not cross-validated) and the DyNetCP model is using NM+1 parameters to predict ~100 data points (It would also be good to say what N and M are for the results here). The GLMCC model has 2 or 3 parameters (if I remember right?).

In the section "Static connectivity inferred by the DyNetCP from in-vivo recordings is biologically interpretable"... I may have missed it, but how is the "functional delay" calculated? And am I understanding right that for the DyNetCP you are just using [w_i\toj, w_j\toi] in place of the CCG?

https://doi.org/10.7554/eLife.95449.2.sa1

Author response:

The following is the authors' response to the original reviews.

We thank the reviewers for the constructive criticism and detailed assessment of our work which helped us to significantly improve our manuscript. We made significant changes to the text to better clarify our goals and approaches. To make our main goal of extracting the network dynamics clearer and to highlight the main advantage of our method in comparison with prior work we incorporated Videos 1-4 into the main text. We hope that these changes, together with the rest of our responses, convincingly demonstrate the utility of our method in producing results that are typically omitted from analysis by other methods and can provide important novel insights on the dynamics of the brain circuits.

> ***Reviewer #1 (Public Review):***
>
> *(1) "First, this paper attempts to show the superiority of DyNetCP by comparing the performance of synaptic connectivity inference with GLMCC (Figure 2)."*

We believe that the goals of our work were not adequately formulated in the original manuscript that generated this apparent misunderstanding. As opposed to most of the prior work focused on reconstruction of static connectivity from spiking data (including GLMCC), our ultimate goal is to learn the dynamic connectivity structure, i.e. to extract time-dependent strength of the directed connectivity in the network. Since this formulation is fundamentally different from most of the prior work, therefore the goal here is not to show the "improvement" or "superiority" over prior methods that mostly focused on inference of static connectivity, but rather to thoroughly validate our approach and to show its usefulness for the dynamic analysis of experimental data.

> *(2) "This paper also compares the proposed method with standard statistical methods, such as jitter-corrected CCG (Figure 3) and JPSTH (Figure 4). It only shows that the results obtained by the proposed method are consistent with those obtained by the existing methods (CCG or JPSTH), which does not show the superiority of the proposed method."*

The major problem for designing such a dynamic model is the virtual absence of ground-truth data either as verified experimental datasets or synthetic data with known time-varying connectivity. In this situation optimization of the model hyper-parameters and model verification is largely becoming a "shot in the dark". Therefore, to resolve this problem and make the model generalizable, here we adopted a two-stage approach, where in the first step we learn static connections followed in the next step by inference of temporally varying dynamic connectivity. Dividing the problem into two stages enables us to separately compare the results of both stages to traditional descriptive statistical approaches. Static connectivity results of the model obtained in stage 1 are compared to classical pairwise CCG (Fig.2A,B) and GLMCC (Fig.2 C,D,E), while dynamic connectivity obtained in step 2 are compared to pairwise JPSTH (Fig.4D,E).

Importantly, the goal here therefore is not to "outperform" the classical descriptive statistical or any other approaches, but rather to have a solid guidance for designing the model architecture and optimization of hyper-parameters. For example, to produce static weight results in Fig.2A,B that are statistically indistinguishable from the results of classical CCG, the procedure for the selection of weights which contribute to averaging is designed as shown in Fig.9 and discussed in details in the Methods. Optimization of the L2 regularization parameter is illustrated in Fig.4 – figure supplement 1 that enables to produce dynamic weights very close to cJPSTH as evidenced by Pearson coefficient and TOST statistical tests. These comparisons demonstrate that indeed the results of CCG and JPSTH are faithfully

reproduced by our model that, we conclude, is sufficient justification to apply the model to analyze experimental results.

> *(3) "However, the improvement in the synaptic connectivity inference does not seem to be convincing."*

We are grateful for the reviewer to point out to this issue that we believe, as mentioned above, results from the deficiency of the original manuscript to clarify the major motivation for this comparison. Comparison of static connectivity inferred by stage 1 of our model to the results of GLMCC in Fig.2C,D,E is aimed at optimization of yet another two important parameters - the pair spike threshold and the peak height threshold. Here, in Fig. 2D we show that when the peak height threshold is reduced from rigorous 7 standard deviations (SD) to just 5 SD, our model recovers 74% of the ground truth connections that in fact *is better* than 69% produced by GLMCC for a comparable pair spike threshold of 80. As explained above, we do not intend to emphasize here that our model is "superior" since it was not our goal, but rather use this comparison to illustrate the approach for optimization of thresholds for units and pairs filtering as described in detail in Fig. 11 and corresponding section in Methods.

To address these misunderstandings and better clarify the goal of our work we changed the text in the Introductory section accordingly. We also incorporated Videos 1-4 from the Supplementary Materials into the main text as Video 1, Video 2, Video 3, and Video 4. In fact, these videos represent the main advantage (or "superiority") of our model with respect to prior art that enables to infer the time-dependent dynamics of network connectivity as opposed to static connections.

> *(4) "While this paper compares the performance of DyNetCP with a state-of-the-art method (GLMCC), there are several problems with the comparison. For example:*
>
> *(a) This paper focused only on excitatory connections (i.e., ignoring inhibitory neurons).*
>
> *(b) This paper does not compare with existing neural network-based methods (e.g., CoNNECT: Endo et al. Sci. Rep. 2021; Deep learning: Donner et al. bioRxiv, 2024).*
>
> *(c) Only a population of neurons generated from the Hodgkin-Huxley model was evaluated."*

(a) In general, the model of Eq.1 is agnostic to excitatory or inhibitory connections it can recover. In fact, Fig. 5 and Fig.6 illustrate inferred dynamic weights for both excitatory (red arrows) and inhibitory (blue arrows) connections between excitatory (red triangles) and inhibitory (blue circles) neurons. Similarly, inhibitory and excitatory dynamic interactions between connections are represented in Fig. 7 for the larger network across all visual cortices.

(b) As stated above, the goal for the comparison of the static connectivity results of stage 1 of our model to other approaches is to guide the choice of thresholds and optimization of hyperparameters rather than claiming "superiority" of our model. Therefore, comparison with "static" CNN-based model of Endo et al. or ANN-based static model of Donner et al. (submitted to bioRxiv several months after our submission to eLife) is beyond the scope of this work.

(c) We have chosen exactly the same sub-population of neurons from the synthetic HH dataset of Ref. 26 that is used in Fig.6 of Ref. 26 that provides direct comparison of connections reconstructed by GLMCC in the original Ref.26 and the results of our model.

> *(5) "In summary, although DyNetCP has the potential to infer synaptic connections more accurately than existing methods, the paper does not provide sufficient analysis to make*

> *this claim. It is also unclear whether the proposed method is superior to the existing methods for estimating functional connectivity, such as jitter-corrected CCG and JPSTH. Thus, the strength of DyNetCP is unclear."*

As we explained above, we have no intention to claim that our model is more accurate than existing static approaches. In fact, it is not feasible to have better estimation of connectivity than direct descriptive statistical methods as CCG or JPSTH. Instead, comparison with static (CCG and GLMCC) and temporal (JPSTH) approaches are used here to guide the choice of the model thresholds and to inform the optimization of hyper-parameters to make the prediction of the dynamic network connectivity reliable. The main strength of DyNetCP is inference of dynamic connectivity as illustrated in Videos 1-4. We demonstrated the utility of the method on the largest in-vivo experimental dataset available today and extracted the dynamics of cortical connectivity in local and global visual networks. This information is unattainable with any other contemporary methods we are aware of.

> ***Reviewer #1 (Recommendations for the Authors):***
>
> *(6) "First, the authors should clarify the goal of the analysis, i.e., to extract either the functional connectivity or the synaptic connectivity. While this paper assumes that they are the same, it should be noted that functional connectivity can be different from synaptic connectivity (see Steavenson IH, Neurons Behav. Data Anal. Theory 2023)."*

The goal of our analysis is to extract dynamics of the spiking correlations. In this paper we intentionally avoided assigning a biological interpretation to the inferred dynamic weights. Our goal was to demonstrate that a trough of additional information on neural coding is hidden in the dynamics of neural correlations. The information that is typically omitted from the analysis of neuroscience data.

Biological interpretation of the extracted dynamic weights can follow the terminology of the shortterm plasticity between synaptically connected neurons (Refs 25, 33-37) or spike transmission strength (Refs 30-32,46). Alternatively, temporal changes in connection weights can be interpreted in terms of dynamically reconfigurable functional interactions of cortical networks (Refs 8-11,13,47) through which the information is flowing. We could not also exclude interpretation that combines both ideas. In any event our goal here is to extract these signals for a pair (video1, Fig.4), a cortical local circuit (Video 2, Fig.5), and for the whole visual cortical network (Videos 3, 4 and Fig.7).

To clarify this statement, we included a paragraph in the discussion section of the revised paper.

> *(7) "Finally, it would be valuable if the authors could also demonstrate the superiority of DyNetCP qualitatively. Can DyNetCP discover something interesting for neuroscientists from the large-scale in vivo dataset that the existing method cannot?"*

The model discovers dynamic time-varying changes in neuron synchronous spiking (Videos 1-4) that more traditional methods like CCG or GLMCC are not able to detect. The revealed dynamics is happening at the very short time scales of the order of just a few ms during the stimulus presentation. Calculations of the intrinsic dimensionality of the spiking manifold (Fig. 8) reveal that up to 25 additional dimensions of the neural code can be recovered using our approach. These dimensions are typically omitted from the analysis of the neural circuits using traditional methods.

> ***Reviewer #2 (Public Review):***
>
> *(1) "Simulation for dynamic connectivity. It certainly seems doable to simulate a recurrent spiking network whose weights change over time, and I think this would be a worthwhile validation for this DyNetCP model. In particular, I think it would be valuable to understand how much the model overfits, and how accurately it can track known changes in coupling strength."*

We are very grateful to the reviewer for this insight. Verification of the model on synthetic data with known time-varying connectivity would indeed be very useful. We did generate a synthetic dataset to test some of the model performance metrics - i.e. testing its ability to distinguish True Positive (TP) from False Positive (FP) "serial" or "common input" connections (Fig.10A,B). Comparison of dynamic and static weights might indeed help to distinguish TP connections from an artifactual FP connections.

Generating a large synthetic dataset with known dynamic connections that mimics interactions in cortical networks is, however, a separate and not very trivial task that is beyond the scope of this work. Instead, we designed a model with an architecture where overfitting can be tested in two consecutive stages by comparison with descriptive statistical approaches – CCG and JPSTH. Static stage 1 of the model predicts correlations that are statistically indistinguishable from the CCG results (Fig.2A,B). The dynamic stage 2 of the model produce dynamic weight matrices that faithfully reproduce the cJPSTH (Fig.4D,E). Calculated Pearson correlation coefficients and TOST testing enable optimizing the L2 regularization parameter as shown in Fig.4 – supplement 1 and described in detail in the Methods section. The ability to test results of both stages separately to descriptive statistical results is the main advantage of the chosen model architecture that allow to verify that the model does not overfit and can predict changes in coupling strength at least as good as descriptive statistical approaches (see also our answer above to the Reviewer #1 questions).

> *(2) "If the only goal is "smoothing" time-varying CCGs, there are much easier statistical methods to do this (c.f. McKenzie et al. Neuron, 2021. Ren, Wei, Ghanbari, Stevenson. J Neurosci, 2022), and simulations could be useful to illustrate what the model adds beyond smoothing."*

We are grateful to the reviewer for bringing up these very interesting and relevant references that we added to the discussion section in the paper. Especially of interest is the second one, that is calculating the time-varying CCG weight ("efficacy" in the paper terms) on the same Allen Institute Visual dataset as our work is using. It is indeed an elegant way to extract time-variable coupling strength that is similar to what our model is generating. The major difference of our model from that of Ren et al., as well as from GLMCC and any statistical approaches is that the DyNetCP learns connections of an entire network jointly in one pass, rather than calculating coupling separately for each pair in the dataset without considering the relative influence of other pairs in the network. Hence, our model can infer connections beyond pairwise (see Fig. 11 and corresponding discussion in Methods) while performing the inferences with computational efficiency.

> *(3) "Stimulus vs noise correlations. For studying correlations between neurons in sensory systems that are strongly driven by stimuli, it's common to use shuffling over trials to distinguish between stimulus correlations and "noise" correlations or putative synaptic connections. This would be a valuable comparison for Figure 5 to show if these are dynamic stimulus correlations or noise correlations. I would also suggest just plotting the CCGs calculated with a moving window to better illustrate how (and if) the dynamic weights differ from the data."*

Thank you for this suggestion. Note that for all weight calculations in our model a standard jitter correction procedure of Ref. 33 Harrison et al., Neural Com 2009 is first implemented to mitigate the influences of correlated slow fluctuations (slow “noise”). Please also note that to obtain the results in Fig. 5 we split the 440 total experimental trials for this session (when animal is running, see Table 1) randomly into 352 training and 88 validation trials by selecting 44 training trials from each configuration of contrast or grating angle and 11 for validation. We checked that this random selection, if changed, produced the very same results as shown in Fig.5.

Comparison of descriptive statistical results of pairwise cJPSTH and the model are shown in Fig. 4D,E. The difference between the two is characterized in Fig.4 – supplement 1 in detail as evidenced by Pearson coefficient and TOST statistical tests.

> ***Reviewer #2 (Recommendations for the Authors):***
>
> *(4) “The method is described as "unsupervised" in the abstract, but most researchers would probably call this "supervised" (the static model, for instance, is logistic regression).”*

The model architecture is composed of two stages to make parameter optimization grounded. While the first stage is regression, the second and the most important stage is not. Therefore, we believe the term “unsupervised” is justified.

> *(5) “Introduction - it may be useful to mention that there have been some previous attempts to describe time-varying connectivity from spikes both with probabilistic models: Stevenson and Kording, Neurips (2011), Linderman, Stock, and Adams, Neurips (2014), Robinson, Berger, and Song, Neural Computation (2016), Wei and Stevenson, Neural Comp (2021) ... and with descriptive statistics: Fujisawa et al. Nat Neuroscience (2008), English et al. Neuron (2017), McKenzie et al. Neuron (2021).”*

We are very grateful to both reviewers for bringing up these very interesting and relevant references that we gladly included in the discussions within the Introduction and Discussion sections.

> *(6) “In the section "Static connectivity inferred by the DyNetCP from in-vivo recordings is biologically interpretable"... I may have missed it, but how is the "functional delay" calculated? And am I understanding right that for the DyNetCP you are just using [w_i\toj, w_j\toi] in place of the CCG?”*

The functional delay is calculated as a time lag of the maximum (or minimum) in the CCG (or static weight matrix). The static weight that the model is extracting is indeed the wiwj product. We changed the text in this section to better clarify these definitions.

> *(7) “P14 typo "sparce spiking" sparse”*

Fixed. Thank you.

> *(8) “Suggest rewarding "Extra-laminar interactions reveal formation of neuronal ensembles with both feedforward (e.g., layer 4 to layer 5), and feedback (e.g., layer 5 to layer 4) drives." I'm not sure this method can truly distinguish common input from directed, recurrent cortical effects. Just as an example in Figure 5, it looks like 2->4, 0->4, and 3>2 are 0 lag effects. If you wanted to add the "functional delay" analysis to this laminar result that could support some stronger claims about directionality, though.”*

The time lags for the results of Fig. 5 are indeed small, but, however, quantifiable. Left panel Fig. 5A shows static results with the correlation peaks shifted by 1ms from zero lag.

> *(9) "Methods - I think it would be useful to mention how many parameters the full DyNetCP model has."*

Overall, after the architecture of Fig.1C is established, dynamic weight averaging procedure is selected (Fig.9), and Fourier features are introduced (Fig.10), there is just a few parameters to optimize including L2 regularization (Fig.4 – supplement 1) and loss coefficient (Fig.1 – figure supplement 1A). Other variables, common for all statistical approaches, include bin sizes in the lag time and in the trial time. Decreasing the bin size will improve time resolution while decreasing the number of spikes in each bin for reliable inference. Therefore, number of spikes threshold and other related thresholds α_s , α_w , α_p as well as $\lambda i \lambda j$, need to be adjusted accordingly (Fig.11) as discussed in detail in the Methods, Section 4. We included this sentence in the text.

> *(10) "It may be useful to also mention recent results in mice (Senzai et al. Neuron, 2019) and monkeys (Trepka...Moore. eLife, 2022) that are assessing similar laminar structures with CCGs."*

Thank you for pointing out these very interesting references. We added a paragraph in "Dynamic connectivity in VISp primary visual area" section comparing our results with these findings. In short, we observed that connections are distributed across the cortical depth with nearly the same maximum weights (Fig.7A) that is inconsistent with observed in Trepka et al, 2022 greatly diminished static connection efficacy within <200μm from the source. It is consistent, however, with the work of Senzai et al, 2019 that reveals much stronger long-distance correlations between layer 2/3 and layer 5 during waking in comparison to sleep states. In both cases these observations represent static connections averaged over a trial time, while the results presented in Video 3 and Fig.7A show strong temporal modulation of the connection strength between all the layers during the stimulus presentation. Therefore, our results demonstrate that tracking dynamic connectivity patterns in local cortical networks can be invaluable in assessing circuitlevel dynamic network organization.

https://doi.org/10.7554/eLife.95449.2.sa0